American Mineralogist, Volume 103, pages 394–411, 2018

A mineralogical archive of the biogeochemical sulfur cycle preserved in the subsurface of the Río Tinto system

David C. Fernández-Remolar[1,*], Neil Banerjee[2], David Gómez-Ortiz[3], Matthew Izawa[4], and Ricardo Amils[5,6]

[1]Department of Computer Science, Electrical and Space Engineering, Luleå University of Technology, Luleå, Sweden
[2]Centre for Planetary Science and Exploration (CPSX), Department of Earth Sciences, University of Western Ontario, 1151 Richmond Street, London, Ontario N6A 5B7, Canada
[3]ESCET-Área de Geología, Universidad Rey Juan Carlos, 28933 Móstoles, Madrid, Spain
[4]Institute for Planetary Materials, Okayama University, Misasa, Tottori, 682-0193, Japan
[5]Planetology and Habitability Department, Center of Astrobiology (INTA-CSIC), Torrejón de Ardoz, 28850 Madrid, Spain
[6]Centro de Biología Molecular Severo Ochoa (CSIC-UAM), Universidad Autónoma de Madrid, Cantoblanco, 28049 Madrid, Spain

Abstract

The search for extinct and extant life on Mars is based on the study of biosignatures that could be preserved under Mars-like, extreme conditions that are replicated in different terrestrial analog environments. The mineral record in the subsurface of the Río Tinto system is one example of a Mars analog site that has been exposed to weathering conditions, including the biogeochemical activity of Fe and S chemolithotrophic bacteria, for millions of years. The SEM-EDAX analysis of different samples recovered in the Peña de Hierro area from four boreholes, ranging from 166 to 610 m in depth, has provided the identification of microbial structures that have affected a suite of hydrothermal minerals (~345 Ma) as well as minerals likely produced by biological activity in more recent times (<7 Ma). The hydrothermal minerals correspond to reduced sulfur or sulfate-bearing compounds (e.g., pyrite and barite) that are covered by bacilli- or filamentous-like microbial structures and/or secondary ferrous carbonates (e.g., siderite) with laminar to spherical structures. The secondary iron carbonates can be in direct contact or above an empty interphase with the primary hydrothermal minerals following a wavy to bent contact. Such an empty interphase is usually filled with nanoscale, straight filamentous structures that have a carbonaceous composition. The occurrence of a sulfur and iron chemolithotrophic community in the Río Tinto basement strongly suggests that the association between sulfur-bearing minerals, dissolution scars and secondary minerals of biological origin is a complex process involving the microbial attack on mineral surfaces by sulfur reducing bacteria followed by the precipitation of iron-rich carbonates. In this scenario, iron sulfide compounds such as pyrite would act as electron donors under microbial oxidation, while sulfate minerals such as barite would act as electron acceptors through sulfate reduction. Furthermore, the formation of siderite would have resulted from carbonate biomineralization of iron chemoheterotrophic organisms or other microorganisms that concentrate carbonate through metabolic pathways. Although the distribution of the mineral biosignatures at depth clearly follows a redox gradient, they show some irregular allocation underground, suggesting that the geochemical conditions governing the microbial activity are affected by local changes associated with the fracturing pattern of the Río Tinto basement. The abundance of sulfur- and iron-bearing minerals in the Mars crust suggests that the Río Tinto mineral biosignatures can be useful in the search for extant and extinct subsurface life on the red planet.

Keywords: Río Tinto, biomineralization, subsurface, Mars

Introduction

The biogeochemical cycling of elements on Earth has occurred for over four billion years (Knoll et al. 2012). Through such a long-term interaction of microbes with minerals, the geosphere has recorded very different components, including structures, fossil bodies, minerals, isotopic fractionation, organic compounds, or biomolecules, that unequivocally evidence a biological origin. While biomolecules and organic compounds provide taxonomic, phylogenic, ecological, and/or metabolic information for the identification of living forms that have produced them (Brocks and Summons 2003), mineral biosignatures provide clues about the metabolic pathways and biogeochemical cycles occurring in Earth's natural systems (Banfield et al. 2001). In this regard, some minerals produced under adverse thermodynamic conditions can form as byproducts of microbial metabolism and can be robust biosignatures. This is the case for the microbial-induced precipitation of siderite by local changes of pH occurring at the microscale under the extremely acidic conditions of the Mars terrestrial analog of Río Tinto (Fernández-Remolar et al. 2012). Consequently, when mineral stability is considered together with geochemical conditions and biological activity in any geochemical system, it

* E-mail: davfer@ltu.se

0003-004X/18/0003–394$05.00/DOI: http://dx.doi.org/10.2138/am-2018-6288

can be used as a good reference for identifying biological activity through mineral diversity. Furthermore, if such geological systems have been identified as suitable analogs of Mars, then the mineral record resulting from interactions with microbiota can be used as conceptual tools to search for life on the red planet.

In this paper, we show how the mineral record has captured the microbial activity in the basement rock of the Río Tinto Mars analog in the Peña de Hierro area during the last 25 millions of years. This has resulted through the synthesis of the knowledge generated in the last two decades through multidisciplinary studies involving the mineralogy, microbiology, geobiology, and geochemistry of such an extreme environment (Fernández-Remolar et al. 2005, 2008, 2011). As one of the main results shows, it has been possible to build strong links between the metabolism of sulfur and iron bacteria (Fernández-Remolar et al. 2008) and the dynamics of sulfur-bearing minerals occurring in the subsurface. Therefore, as a reversed exercise, the formation vs. the destruction of iron and sulfur minerals has provided essential information to understand the microbial processes that have been recorded in the Río Tinto basement on geological timescales. Therefore, such a methodological approach can provide the sulfur and iron mineral cycling to be used as a tool for unlocking geochemical processes and determining whether such cycles were sustained by a putative microbiota on Mars.

Geological settings

The Río Tinto river is a ca. 100 km long river containing a high concentration of heavy metals in solution and extremely acidic conditions (i.e., pH < 3 and Eh > 400 mV). The river is partially sourced by acidic springs located in the Peña de Hierro area, Huelva, southwestern Spain (Fernández-Remolar et al. 2005, 2008). This corresponds to an important mining operation area that comprises the Río Tinto mine district, which is one of the world's largest massive and stockwork sulfide deposits. These mining sites have a long history of activity over the last ca. 5000 years (Davis et al. 2000). Such activity has exposed large outcrops of massive and stockwork sulfides to meteoric water, thereby accelerating metal sulfide oxidation. However, it is a well-known fact that acid mine drainage (AMD) originates from sulfide mineral oxidation catalyzed by iron-oxidizing bacteria that release acid as a byproduct of active metabolism (Nordstrom et al. 2000). Consequently, the extreme conditions of the Río Tinto have been explained so far as a contamination process related to the long mining activity taking place within its catchment area (Davis et al. 2000). However, continuous exploration of the geological, geophysical, and microbiological conditions in the Río Tinto area over the last 15 yr has provided data suggesting that the acidic conditions of the river are not a consequence of the mining activity alone but have remained constant over the last 20 Ma (Fernández-Remolar et al. 2005; Gómez-Ortiz et al. 2014).

Peña de Hierro is an important sulfide ore mining area located at the contact between two different tectonic units belonging to the Iberian Pyrite Belt (IPB). The IPB is a 250 km long and ca. 60 km wide geological unit that forms the northernmost paleogeographic division of the South-Portuguese zone of the Variscan Iberian Massif (Leistel et al. 1998). The presence of rocks formed in an oceanic crust separating the South-Portuguese zone from the rest of the Iberian Massif suggests an exotic origin of this zone relative to the Gondwanan-affinity Iberian Autochthon (Quesada 1991). The stratigraphic record of the Iberian Pyrite Belt can be summarized in three sequences: (1) a Phyllite-Quartzite (PQ) Group of Frasnian to Late Famennian age (Oliveira 1990); (2) a bimodal volcano-sedimentary complex (VSC) ranging in age from Late Famennian to the first part of the Late Viséan (~375–340 Ma), where different metallic ores were formed in response to hydrothermalism and tectonism during the pre-collisional stages of the Variscan orogeny (Leistel et al. 1998; Quesada 1998); and (3) a younger Culm Group (<335 Ma) with turbiditic characteristics (Late Viséan onward) that records syn-orogenic foreland basin deposition during the collisional stage of the Variscan orogeny (Leistel et al. 1998; Quesada 1998). The overall structure of the IPB, as well as that of the entire South-Portuguese zone, corresponds to a huge imbricate fan of thrust sheets rooted in the middle crust (Quesada 1998). Location of the basal detachment within the Late Devonian PQ Group is the reason why no rocks older than this are exposed in the entire region. Significantly, the imbricate thrust structure contains an important oblique-slip component, which is due to the oblique conditions under which the Variscan collision occurred in this part of the orogeny (Quesada 1991, 1998).

The subsurface exploration of the Río Tinto basement in Peña de Hierro has been performed under the umbrella of two main research projects focused on the astrobiology potential of the Río Tinto extreme acidic system. During 2003 and 2004, the MARTE project (Mars Analog and Technology Experiment) simulated a robotic drilling mission to search for subsurface life on Mars (Stoker et al. 2008). For such a purpose, the Río Tinto basement was sampled through different boreholes that principally targeted volcano-sedimentary deposits hosting the metallic orebody. As a result, a total of 350 m of cores were recovered from three drilling targets named BH1, BH4, and BH8 (Fernández-Remolar et al. 2008) that provided the source of information to determine the microbial activity and biogeochemical cycles in the subsurface. In this regard, Fernández-Remolar et al. (2008) identified different subsurface habitats that were characterized by microbial processes controlling the pH and Eh in the Río Tinto Variscan basement.

In the following years, 2011 to 2014, the Iberian Pyrite Belt Subsurface Life (IPBSL) project was the second effort to explore the Río Tinto basement that examined the subsurface of the extreme system through ~1000 m of cores. During 2011, a complete geophysical survey was carried out to detect the occurrence of groundwater as well as the possible location of unknown deep massive and/or stockwork sulfide bodies in the area. Two different methods, Electrical Resistivity Tomography (ERT) and Time Domain ElectroMagnetics (TDEM) (Gómez-Ortiz et al. 2014), were used to sound the Variscan basement. As the presence of both water and metallic bodies greatly modify the electrical properties of the rocks, the methods are especially well suited to the proposed targets. ERT profiles reaching an investigation depth of ca. 200 m (Gómez-Ortiz et al. 2014) revealed the occurrence of two different geoelectrical units: an upper medium-to-high resistivity unit (2000–2500 ohm·m) mimicking the morphology and distribution of the Tournaisian metarhyolites of the VSC that outcrop in the northern (hanging wall) part of Peña de Hierro area, and a lower, low resistivity unit fitting the younger Culm Group that occurs in the southern (foot wall) area. The boundary between both units is defined by a narrow zone dipping north that fits the location of

a mapped major thrust structure that puts into contact the Tournaisian VSC unit and the Culm Group. The massive sulfide ore body mined out at Peña de Hierro was one of several structural imbricates located along this major tectonic fault.

As discussed by Gómez-Ortiz et al. (2014), such a geophysical survey was used to select different drilling targets, based on the distribution of aquifers and metallic orebodies that are the energy source for the microbial community inhabiting the Río Tinto basement. The survey resulted in the selection of two different drilling locations, named BH10 and BH11, for sample collection in the volcano-sedimentary complex hosting the metallic orebodies and the Culm Group, respectively (Fig. 1).

Microbiology of the Río Tinto surface and subsurface

Molecular and microbial ecology studies have shown that ca. 80% of the diversity in the surface environment comprises three bacterial genera that contribute to iron oxidation: *Acidithiobacillus*, *Leptospirillum*, and *Acidiphilium* (González-Toril et al. 2003). Some species, such as *At. ferrooxidans,* oxidize ferrous iron aerobically and reduce ferric iron under anaerobic conditions (Malki et al. 2006; Ohmura et al. 2002), while *Leptospirillum* are aerobic iron oxidizers. Furthermore, *Acidiphilium* has been associated with the formation of siderite by oxidizing organic compounds using ferric iron as an electron acceptor (Fernández-Remolar et al. 2012). *Acidiphilium* can use ferric iron as an electron acceptor in the presence or absence of oxygen (Coupland and Johnson 2008; Malki et al. 2008). In addition, other iron-oxidizing bacteria (i.e., *Ferrovum* spp., *Ferrimicrobium* spp., *Ferroplasma* spp., and *Thermoplasma acidophilum*) or iron-reducing bacteria (i.e., *Ferrimicrobium* spp., *Acidisphaera* spp., *Metallibacterium* spp., and *Acidobacterium* spp.) have been identified in low numbers in the Río Tinto basin (García-Moyano et al. 2012; González-Toril et al. 2003).

Regarding sulfur cycling, only *At. ferrooxidans* can aerobically and anaerobically oxidize both ferrous iron and sulfur. Sulfate-reducing microorganisms that complete the sulfur cycle have been detected in anaerobic areas of the river (García-Moyano et al. 2012; Sánchez-Andrea et al. 2011). In this regard, a comparative analysis of the sediments and the water column of different samples along the Río Tinto river (García-Moyano et al. 2012) has shown much higher levels of biodiversity in the anaerobic sediments than in the corresponding water column. Almost all the identified microorganisms were related to the iron cycle. While the majority of forms have been previously detected and/or isolated (see Amils and Fernández-Remolar 2014, and references therein), some bacteria, such as members of *Actinobacteria*, *Firmicutes*,

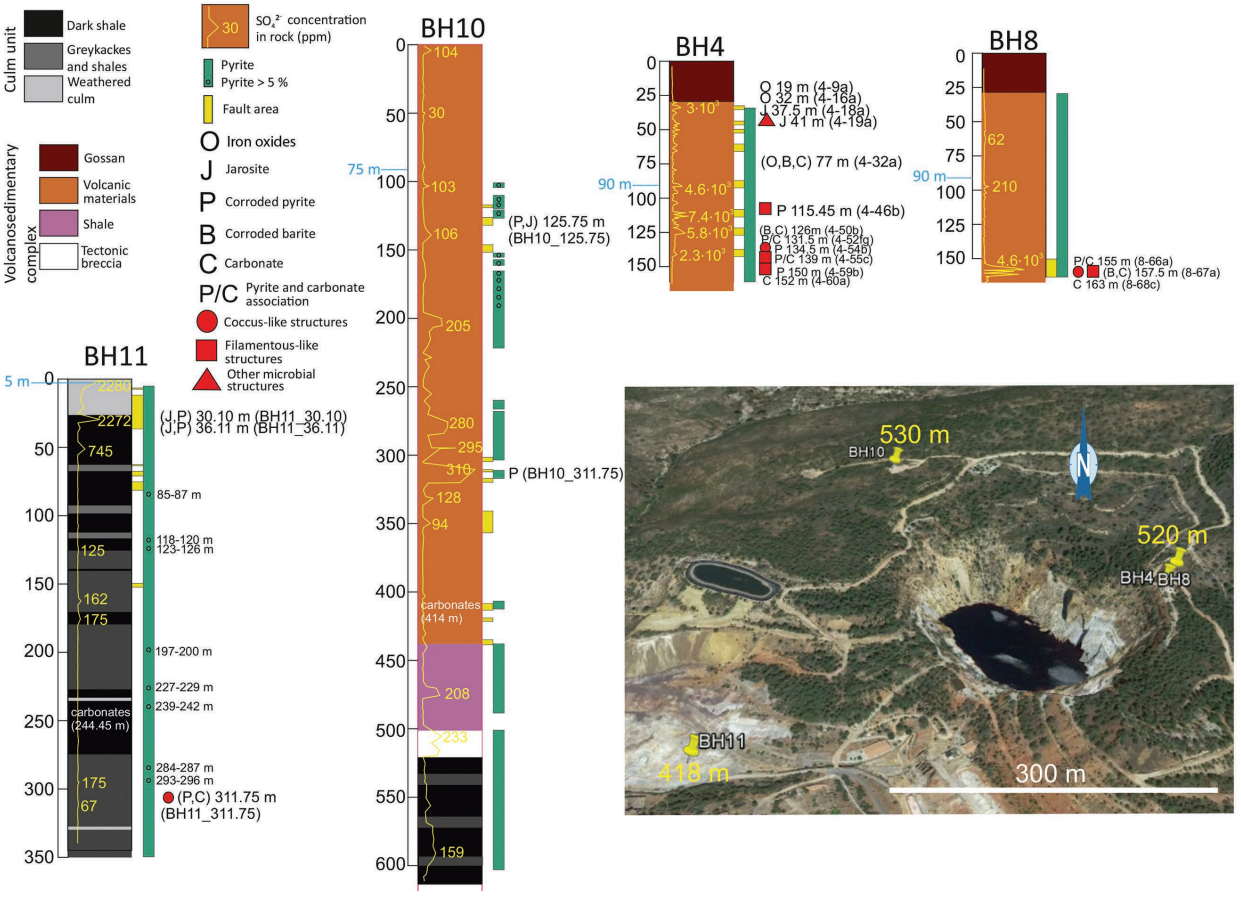


Figure 1. Composite image showing the distribution of boreholes 4, 8, 10, and 11 (BH4, BH8, BH10, and BH11) that drilled to sample the basement of the terrestrial Mars analog of the Río Tinto. The lithology, faults, key minerals, and sulfate content in the rock and the main types of microbial structures are indicated.

Acidobacteria, *Planctomycetes*, and *Chloroflexi* phyla, have been recently discovered in the Río Tinto basin (García-Moyano et al. 2012). An interesting observation from the study of the anaerobic sediments of Río Tinto highlights that under strict anoxic conditions at the sediment bottom, sulfate reduction is a recurrent microbial activity that results from the high concentration of sulfates existing in the system.

Although the Río Tinto environment could be considered a harmful environment for eukaryotic life, it contributes over 60% of the Río Tinto basin biomass (Amaral-Zettler et al. 2002). However, while a great number of eukaryotic species are photosynthetic, fungi are a diverse group of organisms that can play a role in the subsurface of Río Tinto (Oggerin et al. 2013). In this regard, López-Archilla et al. (2005) identified more than 350 fungal isolates, revealing Ascomycetes as the most abundant phylum, while *Basidiomycetes* and *Zygomycetes* accounted for less than 2% of the sequenced isolates.

By using microbiological and molecular techniques on core samples, different bacterial and archaeal forms have been detected at different depths in the subsurface. These techniques included enrichment cultures, 16S rRNA cloning and sequencing, Fluorescence In Situ Hybridization and Catalized Reporter Deposition (CARD-FISH), and the LDChip200 and LDChip300 microsensors (Parro et al. 2008; Puente-Sánchez et al. 2014). The molecular and microbial analyses of the cores suggest that a great portion of the microbial communities in the subsurface are composed of the same microbial forms that are found in the river environment (Amils and Fernández-Remolar 2014). Therefore, the S and Fe compounds in the subsurface are exposed to the same biogeochemical cycles that are ongoing at the surface of the Río Tinto river. As a result, different chemolithoautotrophs were detected, including aerobic and anaerobic pyrite oxidizers, which include anaerobic thiosulfate oxidizers that use nitrate as the electron acceptor as well as sulfate reducers (SRB) and methanogenic Euryarchaeota. Downstream of the metallic orebodies, dissolved sulfate in groundwater was in much higher concentrations that result from the interaction with the pyrite bodies. In this case, microbiological and molecular techniques have shown that sulfate-reducing and methanogenic activity were the main microbial processes occurring along the downstream section of the Río-Tinto Variscan basement. Although dissolved H_2 was lower in BH1 than in BH4 and BH8 (Fernández-Remolar et al. 2008), there was enough to make it available as a microbial electron donor and release methane in concentrations that were several orders of magnitude higher than in BH4 and BH8.

Methods

The geobiological study of the Río Tinto Variscan basement involved a multidisciplinary approach, including a survey of the surface and subsurface (hydro)geology. It was followed by mineralogical, geochemical, and microbiological analysis of samples collected in the subsurface (Amils et al. 2013; Fernández-Remolar et al. 2008). The basement was inspected by geophysical soundings up to a depth of ca. 600 m to recognize the subsurface framework of the aquifers and metallic orebodies (Gómez-Ortiz et al. 2014), which are the essential components controlling the distribution of microbial communities underground. Such information was essential to select the location of the boreholes that sampled the microbial habitats of the Río Tinto basement. As discussed in the geological setting, the samples come from four boreholes, BH4, BH8, BH10, and BH11 (Fig. 1), performed by the MARTE and IPBSL projects that were developed to provide evidence of underground microbial activity in the Río Tinto basement in Peña de Hierro (Amils et al. 2013; Fernández-Remolar et al. 2008).

Boreholes were continuously cored by rotary diamond-bit drilling using a Boart-Longyear HQ wireline system with 60 mm diameter cores. The coolant drilling fluid was well water that was re-circulated to lubricate the perforation bit. Sodium bromide (200 ppm) was added to the drilling fluid as a marker to detect potential contamination in samples. Upon retrieval from the drilling rig, cores were divided into 60 cm length parts, inspected for signs of alteration and stored in boxes for permanent storage and curation in the Instituto Geológico Minero de España (IGME) lithoteque in Peñaroya. Selected cores were deposited in plastic bags, oxygen was displaced with N_2, and the bags were sealed and transported to a field laboratory within 60 min. After drilling, boreholes were cased with PVC tubes with holes at different depths to allow water movement. Upon arrival at the field laboratory, cores were placed in an anaerobic chamber (5% H_2, 95% N_2), logged, and photographed. Aseptic subsamples were obtained by splitting cores with a hydraulic core splitter and drilling out the central untouched portion with a rotary hammer with sterile bits and strict temperature control (40 °C maximum). Rock leachates were produced by adding 5 mL sterile water to 0.5 g of powdered core subsamples and allowing them to stand overnight before filtration through pre-rinsed 0.2 μm nylon filters and analyzed in an Advanced Compact Ion Chromatographer (Metrohm AG). Small fragments of subsurface samples were coated with gold, paladium or osmium for SEM investigation, to recover microscopic and microanalytical information regarding the morphology and composition of the mineral and microbial structures found in the subsurface. Scanning electron microscopy and microanalysis was performed using Jeol JSM-5600 LV equipment coupled to a Cambridge INCAx-sight Electron Dispersive Spectrometer (EDS). SEM data analyses were obtained under beam conditions ranging from 10 to 20 keV accelerating voltage, which provided secondary and BSE images plus EDS/EDAX data that were analyzed using INCA Suite software. Therefore, the samples were prepared in a manner that would only allow for biomineralized structures to be targeted.

Results

Carbon-rich mineralized microstructures

The coupled SEM-EDAX analysis of the borehole samples (Figs. 1–4) is a source of evidence that, when combined with molecular and microbial techniques (Parro et al. 2008; Puente-Sánchez et al. 2014), supports the presence of microbial activity in the Río Tinto basement. The observation of microbial structures in the subsurface samples suggests that there is a link between their morphology and size and their depth and mineralogy. The biggest carbon-bearing microstructures consist of 10–15 μm well-defined disk-like structures that are formed by the combination of two curved bacilli-like structures attached to quartz (Fig. 2a) that are in close association with micrometer-sized, acicular Fe-rich sulfates. Such discoidal structures laterally change to form clusters of smaller ovoidal and elongated units (<10 μm length) (Fig. 2a) occurring at a shallow depth (41 m). In the same depth range, 3.5 to 4 μm oval cells (Fig. 2b) are also found on quartz. In this regard, Fernández-Remolar et al. (2008) report the presence of some large microbial structures, such as filaments, mineralized at 21 m depth that have been characterized as fungal hyphae.

In areas deeper than 100 m, the microbial structures are usually much smaller (<1 μm) and appear in close association with sulfur-bearing minerals. In this regard, there are three main morphologies that include coccus-like, filamentous networks and upright filaments. At 134.5 m depth, colonies of tiny (<1 μm), disperse, spheroidal bodies (Fig. 2c) occur on pyrite surfaces where nanoscale cavities with circular morphology also occur. The same microbial structures have been reported at a depth of 162 m by Fernández-Remolar et al. (2008) growing on similar pyrite surfaces and showing mucilaginous capsule-embedding spheroid rows (Supplemental[1] Fig. 1) in BH8. Very distinctive structures formed by intricate and dense networks of sinuous and overlapping filaments of few tens of micrometers of length have been found at

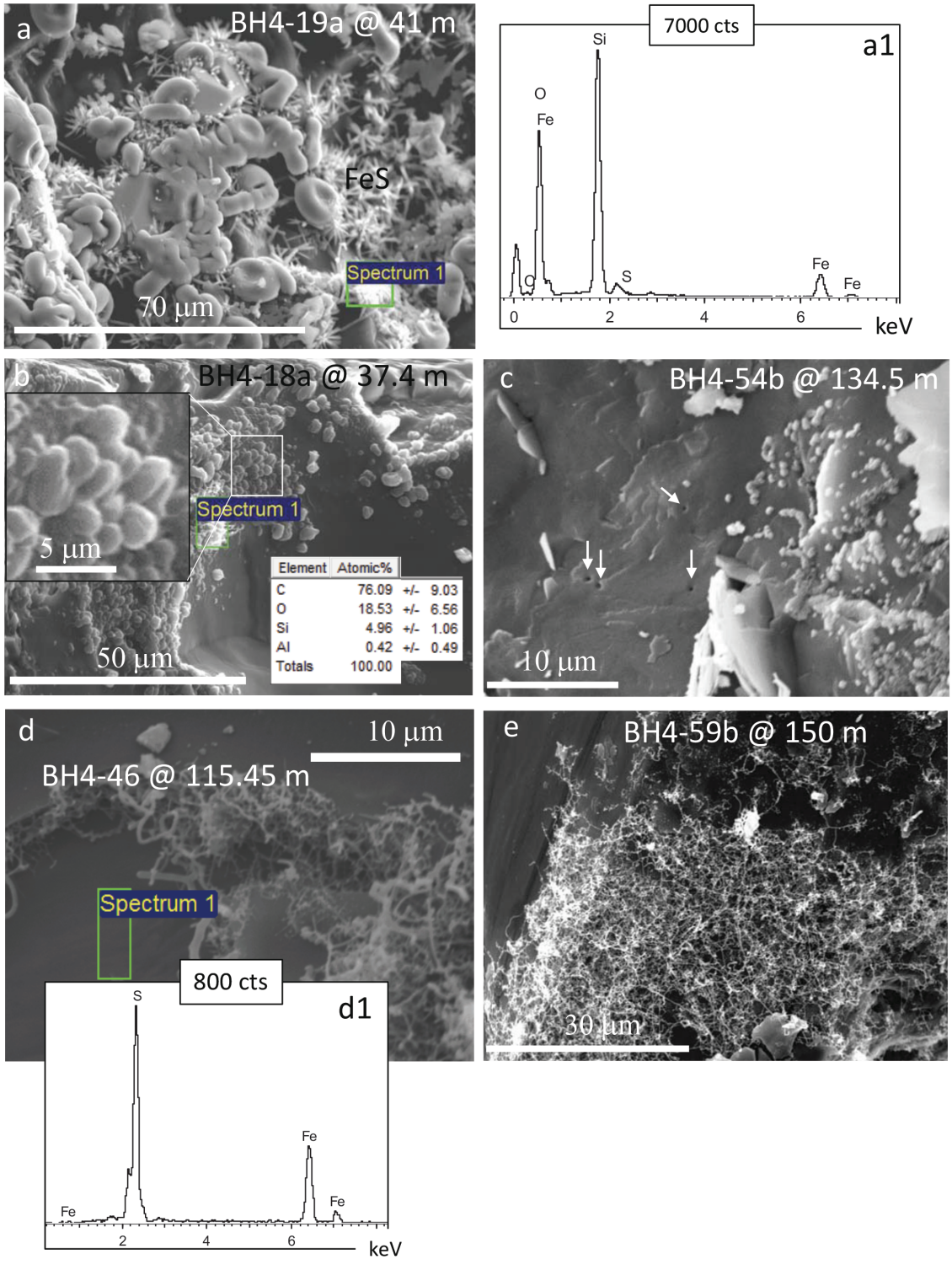


Figure 2. Diverse mineralized microstructures found on the surfaces of quartz and pyrite that show evidence of active mineral attack. (**a**) Discoidal to vermicular carbon-rich structures covering a quartz surface that are associated with Fe sulfates (FeS) in sample 4-19a, found at a depth of 41 m (see main EDAX peaks for S, O, Fe, Si, and C shown in **a1**). (**b**) Oval-like C-bearing bodies spread over a quartz surface in sample 4-18a (37.4 m). (**c**) Carbon-rich microstructures found in sample 4-54b (depth of 134.5 m) associated with nanoscale pits (white arrows), suggesting biomineralized nanobacteria and pits that could be the result of microbial attack. (**d** and **e**) Very dense network of C-bearing sinuous threads resembling exopolymers found on the interior and surface of pyrite (unique peaks of S and Fe in **d1**) in samples 4-46b and 4-59b, at depths of 115.45 and 150 m, respectively. The peak at 2.2 keV corresponds to Au coating for sample preparation.

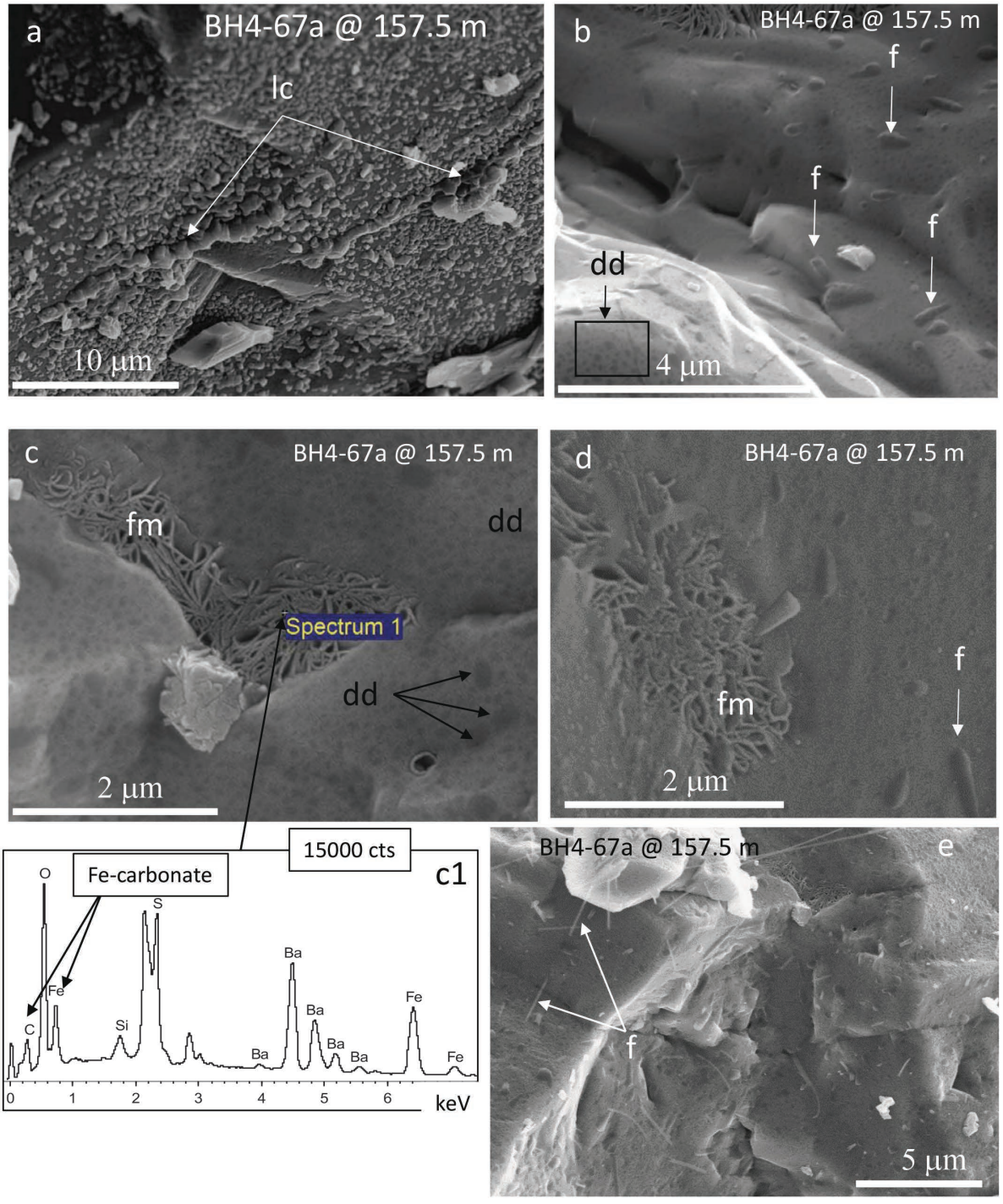


Figure 3. Very distinctive mineralized structures (157.5 m) recovered from BH4, which are associated with barite and pyrite surfaces and where filaments (f) and dark dots (dd) are observed. (**a**) Tightly packed covering of oval-like, C-bearing structures on a pyrite surface found in sample 4-67a that occasionally are arranged forming linear clusters (lc). (**b**) Remnants of carbonaceous straight filamentous microstructures occurring as ovoides to elongated structures (f) on a barite crystal surface in sample 4-67a after being exposed to the SEM electron beam, which suggests the occurrence of organic carbon. (**c**) Same as in **b**, showing the remnants of totally obliterated filaments occurring as dark dots (dd) covering the barite surface (**c1**). (**c1**) EDAX spectrum that suggests the occurrence of filaments mineralized (fm) to Fe-carbonate (EDAX peaks of C, O, and Fe) infilling a micrometer-sized cavity in the barite surface (EDAX peaks of S, O, and Ba). (**d**) SEM image showing the occurrence of similar filaments that have been mineralized (fm) to Fe-carbonates and some carbonaceous remnants (f) of partially obliterated filaments. (**e**) Intact upright filaments (f) covering the barite surface at 157.5 m. These filaments that have been most frequently obliterated to form tiny carbon-rich bodies after being exposed to the SEM beam.

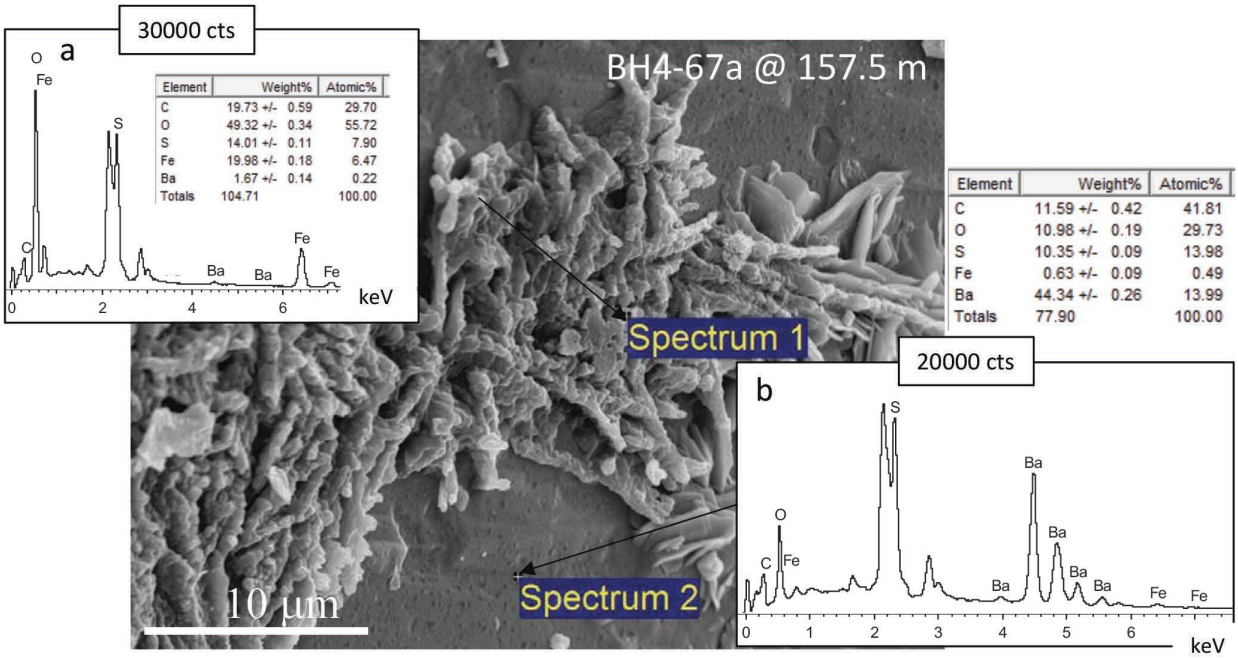


Figure 4. Linear clusters mineralized by Fe-carbonate (siderite) in sample 4-67a (157.5 m). Spectrum **a** shows an elemental composition of the mineralized clusters consistent with a siderite (major X-ray peaks for C, Fe, O, and S) intermixed with small amounts of S-bearing compounds like elemental sulfur or pyrite. Spectrum **b** shows an elemental composition consistent with barite (major X-ray peaks for S, O, and Ba) that is covered by carbonaceous remnants. This is supported by a high concentration of carbon (semi-quantitatively estimated at ~42%, but with significant uncertainty). The presence of a coating of carbon-rich organic matter attenuates the fluorescent X-rays, with a greater attenuation for the lower-energy O and S X-rays than for Ba, which increases the uncertainty in the (semi)quantification by the EDAX software. However, the qualitative interpretation of the X-ray spectra strongly supports the identification of barite with a coating of organic materials. High peak at 2.2 keV placed at the left of S correspond to Au peak coming from the conductive coating. Peaks at 1.7 and 2.7 keV are also from the coating conductive material and correspond to Au and Pd, respectively.

different depths below 100 m (Figs. 2d–2e). They usually emerge from the interior of 10 to 100 μm sized pyrite cavities with straight boundaries (Fig. 2d). Furthermore, the SEM analysis has revealed the presence of compact and dense colonies of 0.5 to 1 μm sized angular-shaped mineralized structures (Fig. 3a) growing on a pyrite surface found at 157.5 m depth. Although such mineralized structures spread uniformly on the mineral surface (Rodriguez-Navarro et al. 2012), they occasionally form linear clusters with signs of mineralization to carbonates (Fig. 3a, Supplemental[1] Fig. 2). Such structures eventually show mucilaginous capsule embedding (Supplemental[1] Fig. 3) as observed in the spheroid rows.

Very distinctive carbonaceous structures were observed in SEM in sample BH4. These structures consisted of 3 to 5 μm long upright filaments above the mineral surface with very thin diameter (ca. 100 nm) that uniformly cover the mineral surface of barite with a separation of 0.3 to 2 μm (Figs. 3b–3e) between two consecutive filaments. The exposure of the filaments to the SEM electron beam has caused a partial or total obliteration of the microstructures, resulting in elongated to equidimensional carbon-rich bodies <2 μm in length (Figs. 3b, 3d, and 3e). In the extreme case of total obliteration of filaments, they occur as a dotted, carbonaceous pattern on the mineral surface (Fig. 3c).

In some circumstances, the structures show mineralization, likely to siderite (Fernández-Remolar et al. 2012), as some isolated clusters of straight and bent filaments that are present on barite surface depressions (Figs. 3c and 3d; Supplemental[1] Fig. 4). Furthermore, this is also the case with the linear clusters of ovoidal bodies mineralized, likely to Fe-carbonate, in sample 4-67a (157.5 m). The elemental composition obtained through EDAX (Figs. 4a and 4b) has shown major elemental peaks for C, Fe, S, and O (Fig. 4a) that support the mineralization to iron carbonate as observed in other similar structures (Supplemental[1] Fig. 2), but also with the presence of S-bearing compounds like elemental sulfur or pyrite resulting from reduction of sulfate in barite. On the other hand, the surface is composed of barite, as evidenced by major peaks of S, O, and Ba (Fig. 4b). Interestingly, the barite surface is densely covered by a dotted pattern of carbonaceous remnants that come from the obliteration of the upright filaments under exposure of the SEM beam, which is supported by a high concentration of carbon of ~42 in atomic percentage (Fig. 4b). The occurrence of carbon-rich organic matter attenuates the fluorescent X-rays, with a greater attenuation for the lower-energy O and S X-rays than for Ba (Goldstein et al. 2003), which increases the uncertainty in the (semi)quantification.

Sulfur and iron minerals

The samples collected at the uppermost part of the Río Tinto Variscan basement show an enrichment in iron oxides and iron sulfates that result from complete oxidation of the orebody under aerobic conditions. Iron oxyhydroxides (hematite and goethite) are

very abundant in association with quartz where microbial attack by chemolithotrophic aerobic communities has taken place (Sand et al. 2001). Hematite and goethite have been identified by SEM-EDAX in the upper part of borehole BH4, in samples 4-9a and 4-16a, collected at a depth of 19 and 32 m, respectively (Fig. 5), occurring as colomorph intergrowths infilling the quartz crosscutting veins of hydrothermal origin (Fernández-Remolar et al. 2008).

In those subsurface areas where the microbial oxidation is ongoing, there is a close association between pyrite and ferric sulfates. Such minerals were found by SEM-EDAX in BH4, BH10, and BH11 at different depths (Fig. 6) occurring as isolated rosettes, amorphous patches or mineral coatings on pyrite. Interestingly, the mineral habit and size is related to the location where the acidic sulfates precipitate with regard to the subsurface water level. Amorphous Fe-sulfate coatings and rosettes (Figs. 6a–6c) have been found below the water table, while large euhedral crystals usually occur above the region under permanent saturation with subsurface solutions (Figs. 6d). In addition, there is a close association between amorphous and rosette Fe-sulfate crystals and the occurrence of evidence of microbial attack. There seems to be different stages of microbial attack, shown first as simple circular and elongate nanoscale pits, arrays of pits and linear scars (Fig. 6b). They evolve to fully corroded surfaces with deep cavities that are filled with carbon-rich materials (Fig. 6a; Supplemental[1] Fig. 5). Furthermore, crystals of primary barite have been found with clear signs of corrosion in BH4 (Fig. 7a) at a depth of 77 m, which is a few meters above the water level. Although barite of hydrothermal origin (~345 Ma) is associated with primary quartz and phyllosilicates as well (Leistel et al. 1998), it co-occurs with secondary iron oxyhydroxides that coat the corrosion scars formed in the barite crystal (Fig. 7a).

In deeper areas, the SEM images show that barite crystals have been exposed to different degrees of chemical dissolution (Figs. 7b and 8). In BH4, at a depth of 126 m, the microscopy analysis

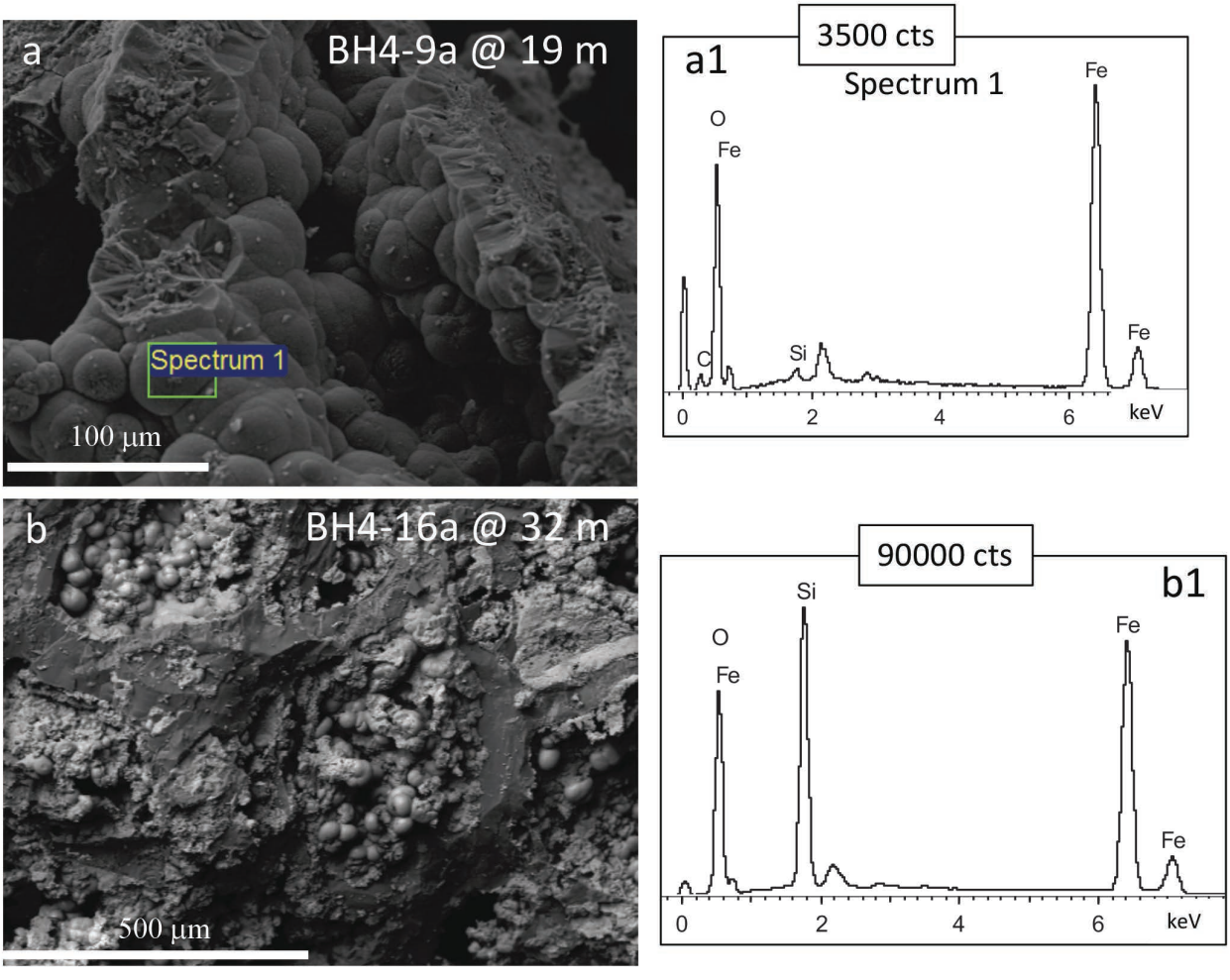


FIGURE 5. Occurrence of ferric oxides detected by EDAX (**a1** and **b1**) in the upper part of borehole BH4, suggesting aerobic conditions for the uppermost region of the Río Tinto basement. (**a**) Sample 4-9a collected at a depth of 19 m, showing colomorphic mineral structures (**a1**) of iron oxides. (**b**) Sample 4-16a recovered at 32 m from BH4 that has a framework of crosscutting veins, in which interspaces are filled with colomorphic iron oxides (**b1**). Spectra **a1** and **b1** were collected from the total area scanned by SEM. The high peak at 2.2 keV corresponds to Au from the conductive coating, which the label has been removed.

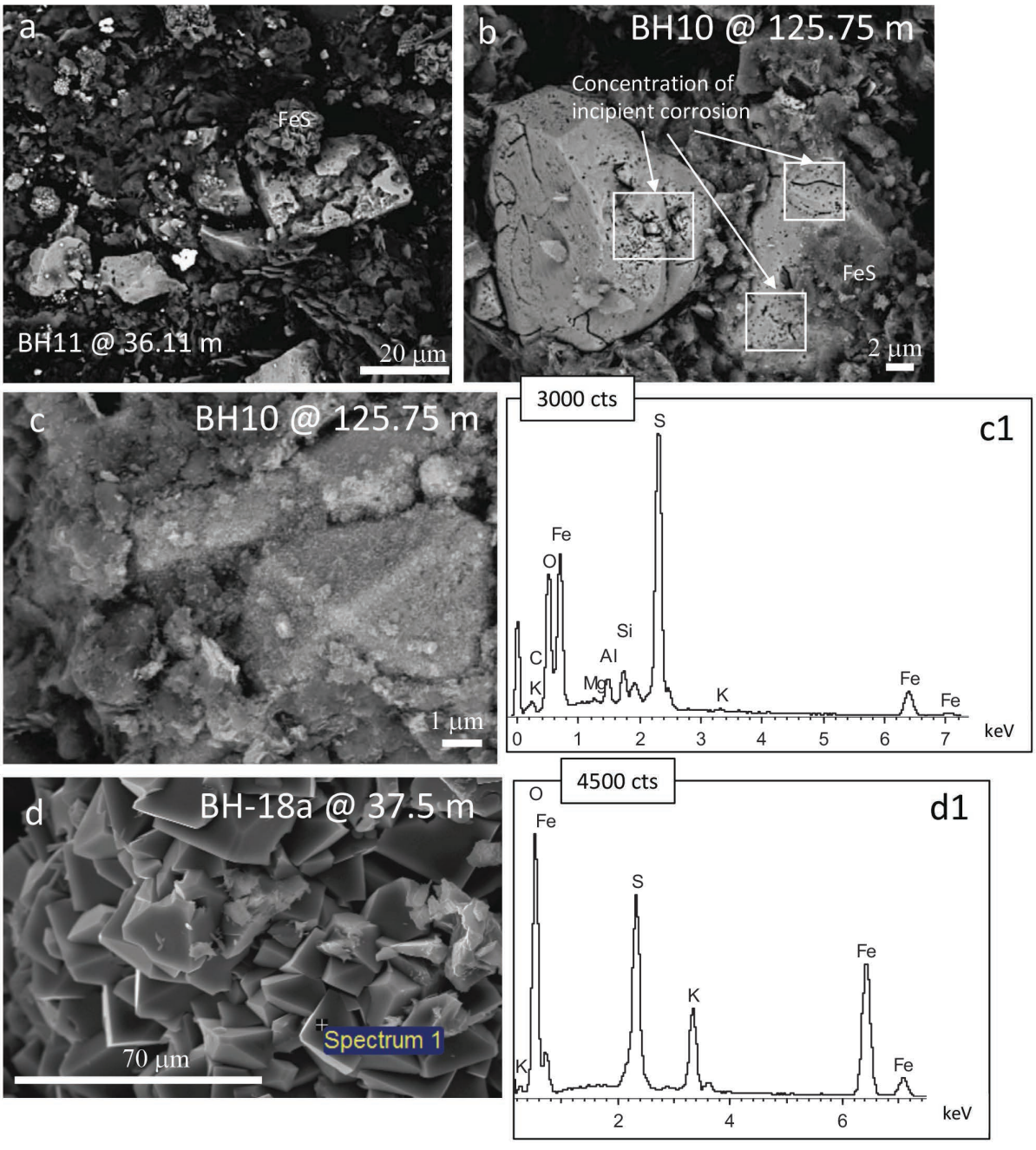


FIGURE 6. Pyrite crystals with clear traces of microbial oxidation and precipitation byproducts as oxidized phases (FeS) that could correspond to ferric sulfates. (**a** and **b**) Samples BH11_36.11 and BH10_125.75 collected in BH11 and BH10 at 36.11 and 125.75 m depths, respectively, showing evidence of advanced and incipient corrosion on the pyrite surfaces by oxidation of sulfur and iron to form rosettes (FeS) and amorphous patches. Squares mark the incipient corrosion (**b**) in pyrites found in sample BH10_125.75. (**c**) EDAX analysis of a full SEM image (**c1**) of a degraded pyrite found in sample BH10_125.75 and completely coated by a ferric sulfate. (**d**) Occurrence of ferric sulfate crystals confirmed by EDAX (**d1**) in sample 4-18a that was collected at a depth of 37.5 m. Peaks at 0.7 and 2.2 keV come from the coating conductive material and correspond to Co and Au, respectively.

of sample 4-50b reveals a prismatic barite crystal with a local attack on areas of the crystal surface followed by precipitation of complex Fe-carbonate spheroids (Fig. 7b). Such a process develops in deeper areas, as shown in samples 4-67a and 8-68c (Fig. 8) that were collected at 157.5 and 163 m, respectively. In sample 4-67a, the barite surface shows an extensively weathered surface with a dotted pattern (Fig. 8a). The barite surface is coated with a carbonate lamina of ~2 μm in thickness (Fig. 8a1) consisting of tightly packed filamentous tabular crystals. Although the siderite lamina coats the barite surface, this occurs above an empty interval of less

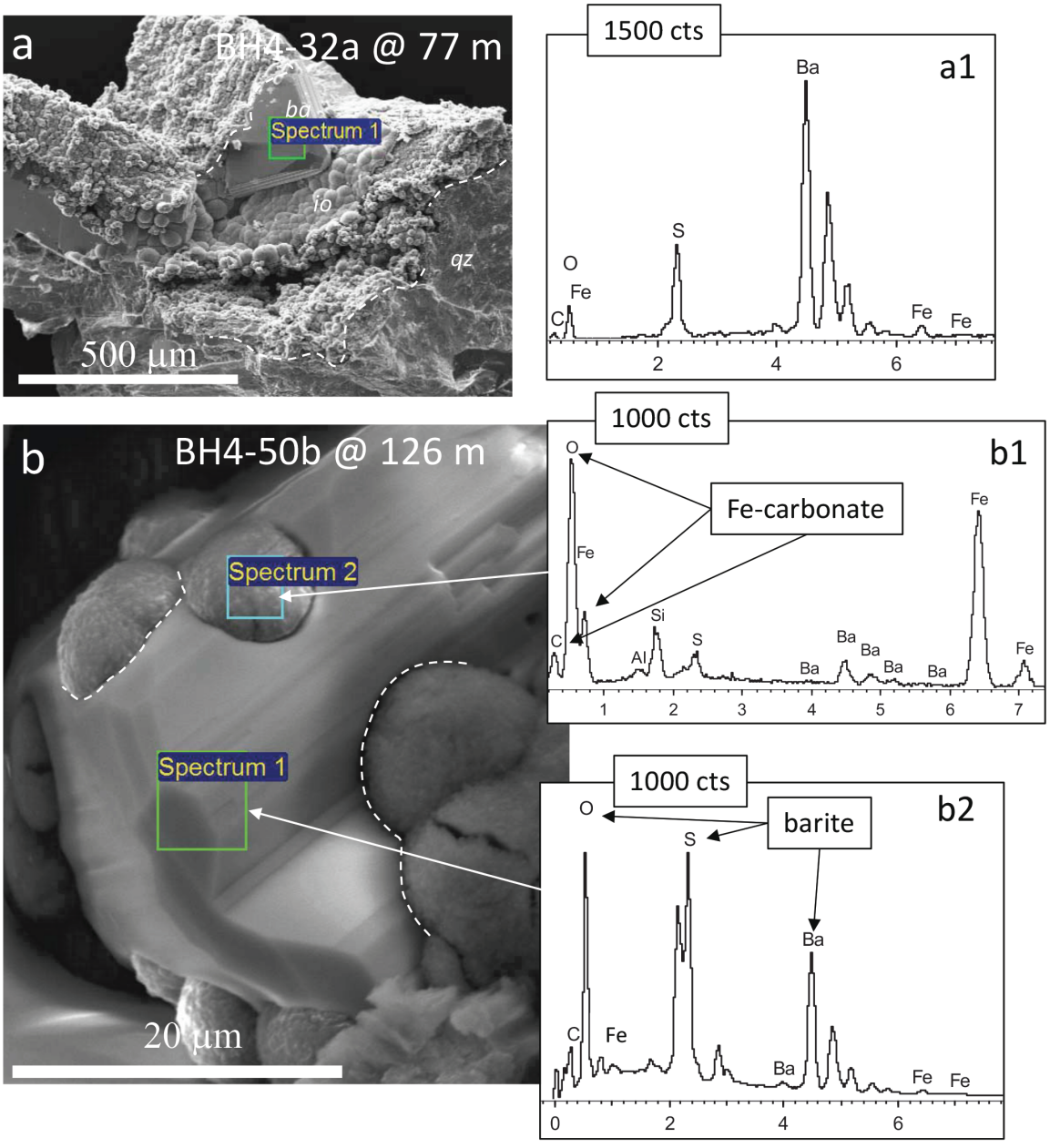


Figure 7. Barite crystals of hydrothermal origin (~345 Ma) found in different areas of the Río Tinto basement that show evident signs of corrosion and precipitation of secondary minerals. (**a**) Association of a corroded crystal of barite (ba) with iron oxides (io), quartz (qz), and Fe-carbonate (see C peak in **a1**), found in sample 4-32a at a depth of 77 m; dashed lines trace the boundary between iron oxides (io) and quartz (qz). (**b**) SEM image of a prismatic barite crystal (**b1**) in sample 4-50b (126 m deep) that has been exposed to local attack at several microsites (some examples of dissolution fronts are traced by dashed lines) followed by the precipitation of complex Fe-carbonate spheroids (**b2**). Unlabeled peak at 2.2 keV placed at the lef of S peak is from the coating conductive material and correspond to Au. Smaller unlabeled peaks starting at 2.9 keV correspond to Pd is from the coating material as well.

than 1 µm of thickness (Fig. 8a). In other cases, the degree of barite corrosion is greater and occurs as isolated fragments of crystals embedded in a mass of 25 µm in size, intergrowing carbonates with filamentous microstructure (Fig. 8b).

The SEM-EDAX study of the subsurface samples has also revealed a close association between siderite, pyrite, and quartz in underground areas below the water table. In this regard, pyrite crystals co-occur with siderite spheroids and disk-shaped laminas (Figs. 9a, 9b, and 9c) that contact the sulfide surface through irregular boundaries and infilling of some cavities. The siderite spheroids can occur in the form of complex aggregates with rosettes fully embedding the pyrite crystals (Fig. 9a). However, some

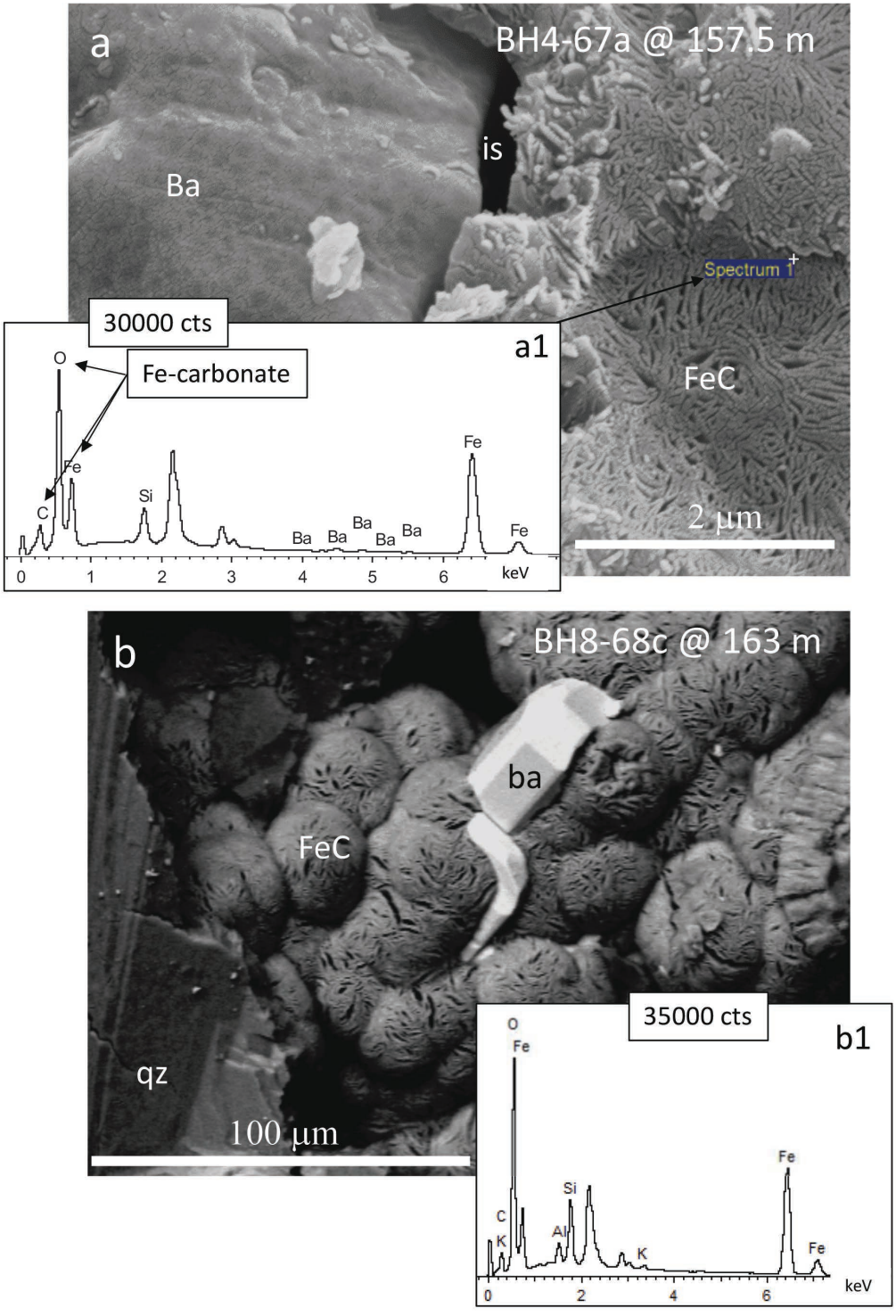


FIGURE 8. Identification of barite crystals in BH4 and BH8 with signs of advanced corrosion. (**a**) Detail of contact between a corroded barite surface (Ba) and an Fe-carbonate ($FeCO_3$) complex labeled as FeC with a filamentous microstructure that are separated by an interspace (is) (sample 4-67a collected at 157.5 m); the barite surface shows a characteristic dotted pattern. (**a1**) EDAX spectrum obtained from the area in **a** showing C, O, Fe, and Ba peaks that are consistent with the occurrence of barite, Fe-carbonate and traces of organic compounds. (**b**) Sample 8-68c collected at a depth of 163 m showing a quartz void (qz) that is filled with remnants of barite crystals (ba) embedded in a matrix of spheroid intergrowths of Fe-carbonates (FeC) with filamentous microfabric. (**b1**) EDAX spectrum of the full image showing C, O, Fe, and Ba peaks consistent with the co-occurrence of barite and Fe-carbonate. Unlabeled peak at 2.2 and 2.9 keV placed at the right of Si peak come from the coating conductive material and correspond to Au and Pd, respectively.

spheroid aggregates can show amorphous microstructure without any evidence of filamentous microstructure. Occasionally, some spheroids seem to fill preexistent cavities that have internal planar sides (Fig. 9c). Interestingly, the siderite frequently shows a disk-shaped appearance when covering silica-rich primary minerals like chlorite (Fig. 9d) and quartz (Fernández-Remolar et al. 2008).

Discussion

Microbial structures

The morphology, size, and/or composition of some microstructures and its association with different mineral surfaces suggests that correspond to microbial remains. They show different degree of biomineralization ranging from carbonaceous to mineralized carbonatic morphologies. In the first group of carbonaceous microstructures, very diverse morphologies are found that comprise the curved bacilli-like structures attached to quartz (Fig. 2a), which laterally change to form clusters of smaller ovoidal and elongated units (<10 μm length). Furthermore, the co-occurrence of disperse, spheroidal bodies (Fig. 2c) and nanoscale cavities with circular morphology on pyrite surfaces show evidence of bacterial cocci that are attacking the sulfide surface. This is also observed in the carbonaceous-rich structures represented by frameworks of sinuous and overlapped filaments (Figs. 2d–2e), which resemble bacteria exopolysaccharide (EPS) and filamentous structures described by Uwins et al. (1998). They usually emerge from the interior of 10 to 100 μm sized pyrite cavities with straight boundaries (Fig. 2d) that suggest an intensive microbial attack along crystallographic planes or structural weakness through the oxidation of sulfide (Welch and Vandevivere 1994; Zhou et al. 2011). In addition, the occurrence of upright carbonaceous filaments that uniformly cover barite surfaces (Figs. 3b–3e) suggests that they might be filamentous bacteria, which obtain energy through metabolizing sulfate ions. In this regard, the occurrence of corroded surfaces with deep cavities that are filled with carbon-rich compounds (Fig. 6a; Supplemental[1] Fig. 5) suggests that the microbial attack on pyrite is also an oxidative process that has been recorded as ferric sulfates.

A second group of structures that are associated to microbial morphologies show mineralization to Fe-carbonates. This is the case of ovoidal microstructures resembling coccus bacterial morphologies that sometimes occur as linear clusters (Figs. 3a; Supplemental[1] Figs. 2 and 3) of ovoid-like units, which are mineralized to Fe-carbonate as shown in EDS spectra. Similar microstructures with linear arrangement (Fig. 4) could correspond to the mineralization to carbonate of primary filamentous microbes. In addition, other structures of bigger size, while cannot be considered as the mineralization of microbial cells, they could be the result of the microbial metabolism of SRB. They correspond to complex Fe-carbonate spheroids (Figs. 7c, 8b, and 9a–9d) that infill voids formed in the mineral surfaces, which formation is discussed below.

Biogeochemical processes

The distribution of iron and sulfur compounds provides essential information with regard to the biogeochemical processes that have been operating over the most recent millions of years in the Río Tinto subsurface (Essalhi et al. 2011; Fernández-Remolar et al. 2008). Such activity has been recorded in the surface as different gossan and terrace levels that are mainly composed of iron oxyhydroxides with trace levels of sulfates (Fernández-Remolar et al. 2005). The SEM-EDAX analysis of the samples occurring in shallower areas of the Río Tinto Variscan basement supports that the main process was led by oxidative and acidic conditions. This is the paradigmatic case of the enrichment in iron oxyhydroxides (Figs. 1 and 5) at the vadose area of the subsurface. However, oxyhydroxide formation took place during mineral maturation of the secondary acidic sulfates (Fernández-Remolar et al. 2011), which originated from a complex, direct, and indirect microbial attack to the pyrite (Sand et al. 2001) as shown in the following reactions:

$$FeS_2 + H_2O + 3.5\ O_2 \rightarrow Fe^{2+} + 2\ SO_4^{2-} + 2\ H^+$$
$$Fe^{2+} + ¼\ O_2 + H^+ \rightarrow Fe^{3+} + ½\ H_2O$$
$$FeS_2 + 14\ Fe^{3+} + 8\ H_2O \rightarrow 15\ Fe^{2+} + 2\ SO_4^{2-} + 16\ H^+.$$

As a result, the biooxidation process acidifies the incoming meteoric solutions (pH 5.5 to 6) that are oversaturated with SO_4^{2-} and Fe^{3+} that have been interacting with the sulfide orebodie along the last 25 Ma (Essalhi et al. 2011). Under the surface and subsurface oxic areas of Río Tinto, the main minerals that precipitate are jarosite and schwertmannite (Fernández-Remolar et al. 2005). Under these conditions, the formation of iron oxyhydroxides in the gossan upper unit and terraces is the result of a complex diagenesis of the acidic sulfates that combines mineral dehydration and exposure to mild acidic meteoric waters. Consequently, the final mineral phases are the iron oxyhydroxides that are favored under a pH ranging from mildly acidic to alkaline. Assuming that schwertmannite is the main mineral phase that precipitates out from the acidic solutions (Burton et al. 2008; Peretyazhko et al. 2009), the following reaction expresses the maturation process of the acidic product to iron oxyhydroxides:

$$Fe_8O_8(OH)_{5.5}(SO_4)_{1.25} + 2.5\ H_2O \rightarrow$$
$$1.25\ SO_4^{2-} + 8\ FeOOH + 2.5\ H^+.$$

Therefore, the occurrence of the iron oxyhydroxides at the top of the iron sulfides is a relic of the ancient microbial activity when the aquifer water table was in shallower areas of the basement that contains sulfides in form of massive orebodies or disseminated pyrite from surface areas up hundreds of meters deep (Gómez-Ortiz et al. 2014). After migrating downward by different geological processes, the acidic sulfates were precipitated and exposed to a combined process of dehydration and ion transportation by meteoric solutions (Fernández-Remolar et al. 2005). Such a mechanism is the same as for the formation of the iron-rich terraces. These were sedimentary bodies originally formed by ferric sulfates that, after being exposed to meteoric waters as a consequence of the river entrenchment, evolved to deposits composed of iron oxyhydroxides.

The association of microbial bodies with iron oxyhydroxides with a size of 15 to 3.5 μm (Figs. 2a and 2b) supports the existence of eukaryotic and bacterial aerobic activity, which promotes acidification under the oxidation of iron sulfides. This is also consistent with the detection of crystalline ferric sulfates (Figs. 2a and 6c) that is the result of precipitation from acidic solutions above the water table. Interestingly, both ferric sulfate structures, including star-like clusters of fibers (Fig. 2a) and rhomboids (Fig. 6c), are formed on quartz mineral surfaces. This finding suggests that dissolved ferric sulfates precipitated from migrating fluids along

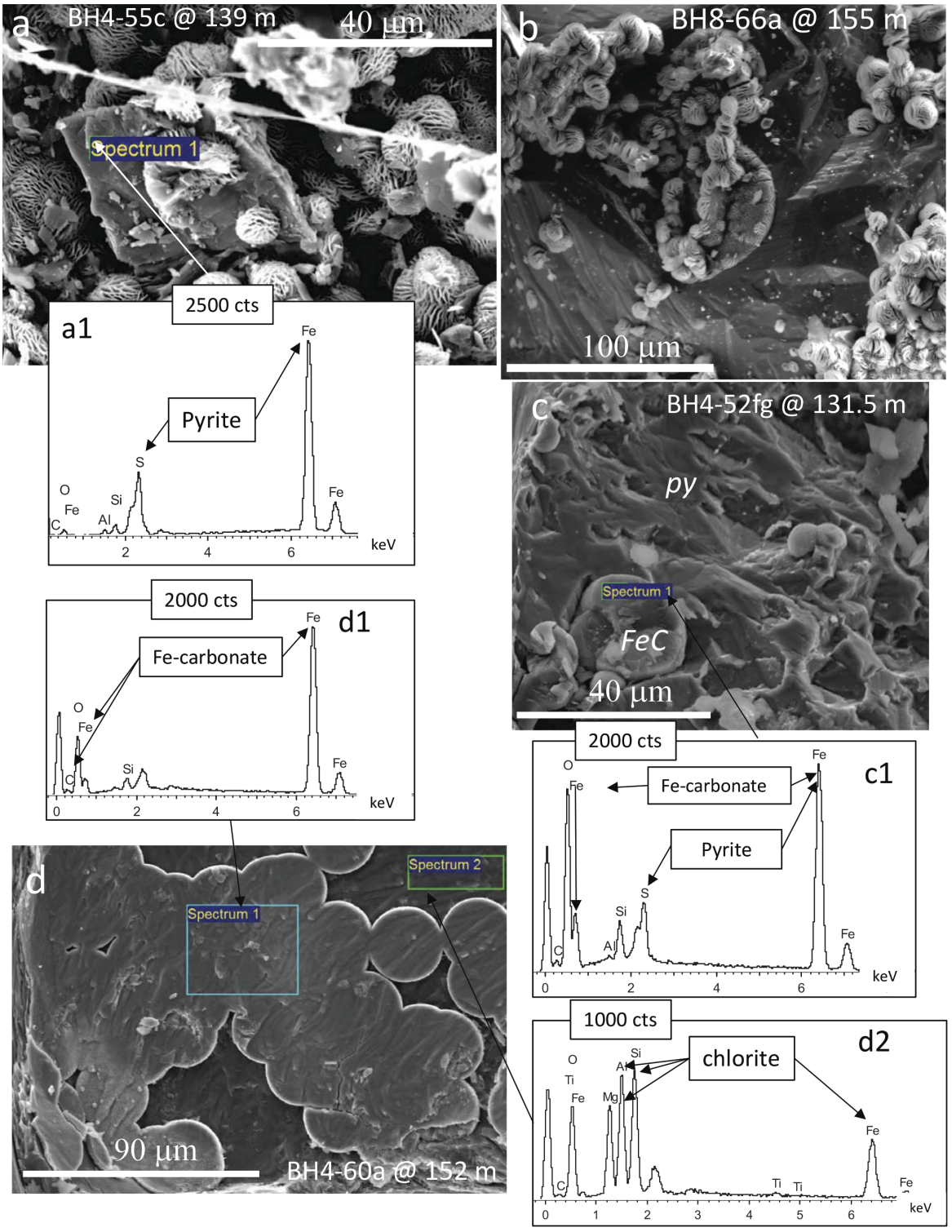


FIGURE 9. Association of Fe-carbonate with pyrite and quartz in deeper regions of the Río Tinto basement in boreholes BH4 and BH8. (**a**) Sample 4-55c collected at 139 m that shows a pyrite crystal embedded in a mass of complex Fe-carbonate spheroids (**a1**); while the pyrite rhombohedrum has an irregular surface, the Fe-carbonate spheroids do not intrude into the sulfide crystal. (**b**) Fe-carbonate spheroids and disk-shaped laminar Fe-carbonate growing on a pyrite crystal, observed in sample 8-66a at 155 m. (**c**) Sample 4-52fg collected at a depth of 131.5 m displaying spheroidal Fe-carbonate (FeC) that grows on a pyrite surface (py) with no evidence of attack and intrusion by the carbonate. (**c1**) EDAX spectrum of an Fe-carbonate spheroid that is shaped by a faceted void of the pyrite surface. (**d**) Sample 4-60a (152 m depth) showing an amalgamation of disk-shaped laminas of Fe-carbonate (**d1**) covering a chlorite rich matrix (**d2**).

the vadose area due to supersaturation, where microbial activity played an indirect role. Furthermore, the formation of the ferric sulfates could also be related to the maturation processes leading to oxyhydroxide compounds. Such processes include the release of SO_4^{2-} and different cations that are mobilized by meteoric waters following a seasonal input (Fernández-Remolar et al. 2003; Gómez-Ortiz et al. 2014). The chemical conditions of the solutions that were acting in the oxic region of the basement have been recorded in the form of dissolution surfaces affecting minerals with low solubility constants, such as barite (Fig. 7a). In sample 4-32a, collected above the water table at 77 m (Fig. 1), barite and quartz crystals have been exposed to a planar dissolution that is followed by the massive formation of iron oxyhydroxides on the dissolution surface. Whether or not acidic sulfates could be a phase transition to iron oxyhydroxides, the dissolution of barite and quartz requires strongly acidic solutions that would be followed by the precipitation of iron-bearing minerals. Barite dissolution is favored by low pH solutions as follows:

$$BaSO_4 + H_3O^+ \rightarrow HSO_4^- + Ba^{2+} + H_2O.$$

Under such acidic and oxic conditions found in the Río Tinto Variscan basement, the optimal dissolution of barite would have occurred at an acidic pH. In this regard, the dissolution of quartz along the same dissolution front, as suggested by the occurrence of iron oxyhydroxides following the same surface that is dissecting the quartz and barite crystals (Fig. 7a), should result of a very aggressive dissolution occurring under a pH ranging between 0 and 2.5 and an high temperature (90–100 °C) that can be reached during the oxic oxidation of the massive sulfides in the subsurface (Crundwell 2014; Leybourne et al. 2009).

Below the water table, there is clear evidence of microbial attack on the pyrite surfaces that come together with rosettes and amorphous patches of iron sulfates (Figs. 6a–6c). The co-occurrence of the carbon-rich compounds inside the corrosion cavities with patchy ferric sulfides and microbial fabrics (e.g., pits, linear to sinuous corrosion) on the pyrite surface strongly suggests an extensive microbial attack that is the source of the acidic conditions observed in BH11 (pH < 3.5, Eh > 450 mV). This corrosion process could also have been driven by abiotic mechanisms discussed by Edwards et al. (1999). However, under acidic conditions, where oxygen is inhibited as an oxidation agent, the pyrite corrosion is driven by the combination of direct and indirect oxidation mechanisms that are triggered by microbial activity (Sand et al. 2001). Consequently, the main biogeochemical processes occurring in the upper acidic and oxic region of the Río Tinto Variscan basement correspond to the precipitation and/or remobilization of sulfate minerals in the vadose area and pyrite bio-oxidation. Both processes release sulfate and ferric iron to deeper regions that can eventually be used as electron acceptors in different metabolic pathways that involve pyrite oxidation by ferric iron and sulfur reduction (Fernández-Remolar et al. 2008).

In deeper regions of the Río Tinto subsurface, the association of barite euhedral crystals with spheroidal to laminar siderite with filamentous fabric and microbial structures (Figs. 7c and 8) strongly suggests that siderite is the final component of a process started by the microbial attack on the barite surface. Regardless of whether the sulfate reduction is a common process in the anaerobic regions of terrestrial crust, as in the Río Tinto subsurface (Fernández-Remolar et al. 2008), little has been reported concerning barite as a potential electron acceptor. In this respect, Bolze et al. (1974) describe the microbial mobilization of barite when sulfur-reducing bacteria are grown with powdered minerals under anaerobic conditions. The occurrence of upright filaments (Supplemental[1] Fig. 6) that have been obliterated during the EDS analysis to bacterial remnants by the electron beam (Figs. 3c–3e) suggests that SRB are currently mobilizing barite in the anaerobic regions of the Río Tinto subsurface. This is supported by the occurrence of such filaments that are growing upright on the barite surface and that are filling the empty interval separating both siderite and barite as shown in Figure 8a. Consequently, the sulfate reducers promote the generation of S mobilization fronts in barite that approach a spherical morphology (Fig. 7b). However, sulfur mobilization recorded in the form of siderite with a microbial-like microstructure (Figs. 3c–3d, 4c, and 7a) suggests that some additional microbial process involves carbonate biomineralization. This could be the result of the oxidation of the organic compounds produced by the SRB that could be metabolized by chemoheterotrophic microbes, such as *Acidiphilium* sp. and *Tessarococcus lapidicaptus,* and promoting the precipitation of siderite under anaerobic conditions. Both microbes have been reported to produce siderite in the anaerobic areas of Río Tinto, including the basement (Fernández-Remolar et al. 2012; Sánchez-Roman et al. 2014, 2015). However, the formation of carbonate following iron reduction requires continuous support of ferric iron, which is highly available in the surface environment of Río Tinto but not in the subsurface. While ferric iron could be supplied from the surface by the mobilization by oxic waters through faults, carbonate could be produced directly from the activity of SRB (Castanier et al. 1999; Baumgartner et al. 2006). Therefore, carbonate could be produced by SRB respiration, in which an organic substrate is metabolized, after pH increase by local concentration of HCO_3^- at the microscale (Baumgartner et al. 2006):

$$SO_4^{2-} + 2\ (CH_2O)\ (\text{organic matter}) + Fe^{2+} \rightarrow FeCO_3 + CO_2 + H_2S + H_2O$$

where pyrite could be secondarily formed under the following process (Drobner et al. 1990; Fernández-Remolar et at. 2008):

$$2\ H_2S + Fe^{2+} + \tfrac{1}{2}\ O_2 \rightarrow FeS_2 + 2\ H^+ + H_2O.$$

Interestingly, the microbial reduction of sulfate in barite could also be mediated by using methane as a substrate (Zhu and Dittrich 2016). As methane has been reported in the Río Tinto Variscan basement (10–95 ppm in subsurface waters, Fernández-Remolar et al. 2008), it could be an additional source of energy used by SRB in the following reaction:

$$CH_4 + BaSO_4 + Fe^{2+} \rightarrow FeCO_3 + H_2S + Ba^{2+} + H_2O.$$

In both cases, the formation of the siderite laminar and spheroidal structures (Supplemental[1] Fig. 7) can be explained as the growth of the microbial colony into the barite crystal by facilitating the precipitation of ferrous carbonates (Fernández-Remolar et al. 2012; Sánchez-Roman et al. 2014). Carbonate growth would proceed through sulfate mobilization and reduction along the

dissolution fronts driven by the microbial dynamics (Supplemental[1] Fig. 7). As the mobilization process is proceeding, siderite mineralization would occur in the external part of the colony where HCO_3^- anions would migrate and concentrate along a pH gradient (Fig. 10) which is increased toward the microsites where bicarbonate is produced through the microbial oxidation of organics (Fernández-Remolar et al. 2012). Such a pH gradient occurring at microscale would be created by the overconcentration of organic acids that are used by bacteria to mobilize ions from mineral surfaces (Bebié and Schoonen 2000).

Interestingly, the collection of rocky samples in deep areas of the Río Tinto subsurface has provided some evidence of mineral microbial corrosion. This is the case for the occurrence of microbial structures co-occurring with microfabrics ranging from nanoscale corrosion traces to microcavities of tens of micrometers (Welch and Vandevivere 1994; Zhou et al. 2011) occupied by biomineralized microbial structures (Figs. 2c–2e and 4a–4b) found in anoxic regions of the subsurface below 115 m depth. They occur in three different settings as follows: (1) nanoscale pits associated with coccus-like microbial bodies (Fig. 2c); (2) tens of micrometers-sized elongated pyrite cavities with straight boundaries occupied or associated with dense networks of filamentous C-rich structures of EPS (Figs. 2d–2e); and (3) equidimensional cavities (<5 μm) infilled with clusters of coccus-like microbial bodies (Figs. 4a–4b) at greater depth (311.75 m).

The correlation between the microbial structures and the corrosion microfabrics affecting the pyrite surface suggests that the microbial communities utilize different approaches for corrosion. While the coccus-like microbes produce microfabrics on the mineral surface going from nanoscale pits to equidimensional cavities, the filamentous networks forming biofilms show an intensive microbial attack along crystallographic planes or structural weakness in the mineral. As there is no mineral byproduct associated with the corrosion microfabrics, it is difficult to determine the metabolic process involved in pyrite degradation, if any. The corrosion process could correspond to pyrite oxidation under anaerobic conditions, which is mediated by the indirect biooxidation of sulfide (Sand et al. 2001). This agrees with the occurrence of Fe^{3+} and SO_4^{2-} (Fig. 1) (Fernández-Remolar et al. 2008), which show average concentrations of 4 and 2.5 mM, respectively, in the subsurface solutions from areas deeper than 110 m from BH4, BH8, and BH10. Therefore, it is very likely that under anaerobic conditions, the formation of ferric sulfates are inhibited, and ferric sulfates would not form as has been observed in the oxic areas of the aquifer where the microbial corrosion microfabrics are associated with ferric sulfate patches (Figs. 6a–6c).

As indirect microbial oxidation of pyrite produces 14 mol of H^+ for each mole of pyrite (Sand et al. 2002), the subsurface solutions should become extremely acidic. However, this is not the case because where the corrosion microfabrics occur, the pH of solutions is neutral. The absence of acid fluids could be related to the production of hydrogen that has been detected in the anoxic regions of the Río Tinto basement (Fernández-Remolar et al. 2008). The production of hydrogen could be directly linked to pyrite attack by protons that have been previously released through the indirect biooxidation of pyrite. This could occur as a secondary biogeochemical pathway expressed with the following reaction (Rickard and Luther 2007):

$$FeS_2 + H^+ \rightarrow S^{2-} + Fe^{3+} + \tfrac{1}{2}\, H_2$$

where the protons would be released by anaerobic biooxidation.

Furthermore, the continuous supply of ferric iron to the anaerobic area of the basement could also be from the migration of shallow solutions through faults. Such a process would be greatly accelerated during the wet season (Fernández-Remolar et al. 2003) that supplies meteoric waters enriched with oxidized compounds from the vadose area. This agrees with the occurrence of fractures and faults in the locations where the sulfate and ferric iron concentrations are increased (Fig. 1).

In this context, the co-occurrence of spheroidal siderite with pyrite that shows clear signs of corrosion (Figs. 9a and 9d) could be a consequence of organic oxidation using SO_4^{2-} as the electron acceptor. In this case, the anaerobic formation of siderite would come from the release of Fe^{2+} through the pyrite oxidation or degradation. As has been reported for chemoheterotrophic bacteria like *Acidiphillium* sp. occurring in the river (Fernández-Remolar et al. 2012; Sánchez-Roman et al. 2015), Fe-carbonates can form by the oxidation of organic matter using Fe^{3+} as electron acceptor. In this regard, siderite precipitate could be directly formed through the heterotrophic release of HCO_3^- when organic compounds are available. While siderite formation could be formed in the aerobic Río Tinto solutions that show an average Fe^{3+} concentration of ~15 mM, it could also be precipitated in the subsurface through the release of ferrous iron by microbial oxidation of pyrite. This could be the case for the presence of disk-like siderite structures on silicic minerals, such as quartz and chlorite (Figs. 9b–9c), which come together with phosphate-bearing compounds, as described by Fernández-Remolar et al. (2008).

Both processes, including the sulfate reduction from barite and the pyrite anaerobic oxidation, require ion mobilization from the mineral surfaces to be available for microbial metabolism. Although there are different mechanisms used by the microbes (Bebié and Schoonen 2000), the high concentration of organic acids like oxalates (>2 ppm) at some depths of the basement unaffected by faulting suggest that organic acids are used to mobilize ionic substrates (e.g., SO_4^{2-}) to sustain chemolithotrophic metabolism. In this context, the overconcentration of organic acids that have been derived from the interaction between microbes and the lithosphere would be a complementary set of biosignatures of cryptic life for any planetary body.

IMPLICATIONS

The two main hydrothermal scenarios for the possible origin of life on Earth, that of vents on the ocean floor and that of volcanic fields at the surface, are also found on Mars (Deamer and Damer 2017; Michalski et al. 2017; Sholes et al. 2017). Under these circumstances, the geochemical processes occurring in the hydrothermal systems of early Mars under a higher concentration of Fe and S (Barlow 2008; King and McLennan 2010) very likely favored the emergence of chemical cycles mimicking some biochemical pathways found in chemoauthotrophic organisms (Wächtershäuser 1992). Therefore, the possible existence on Mars of a mineral sulfur/iron-energy deriving Earth-like microbial life would have even been more probable than on Earth. Thus, the oxidative formation of pyrite (FeS_2) from hydrogen sulfide volatiles (HS^-, H_2S)

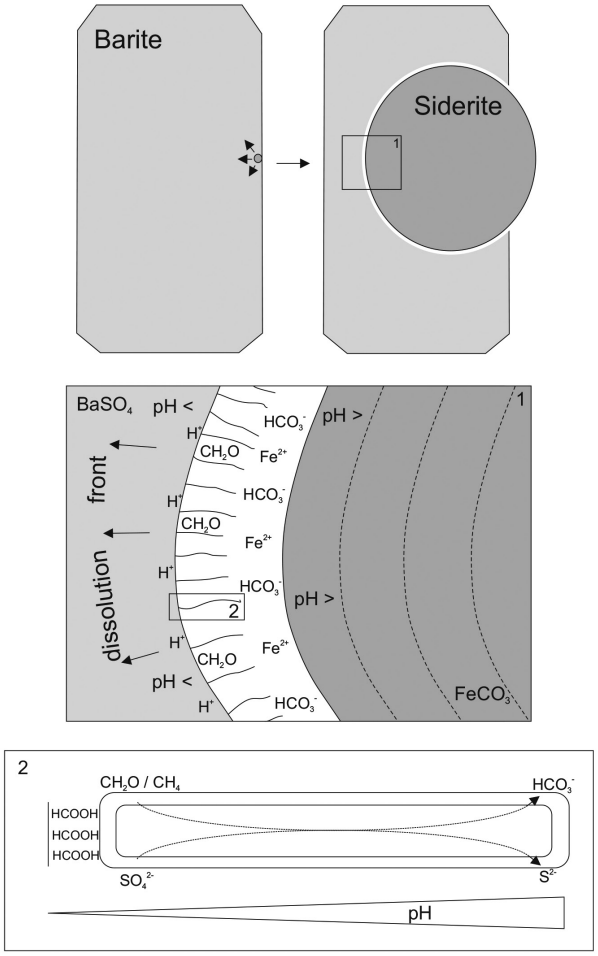


Figure 10. Drawing outlining the microbial attack on a sulfate surface through the mobilization of sulfate anion to sulfide by SRB from the barite surface that results in the formation of Fe-carbonate. The sulfate would mobilize entry into the metabolic machinery by acidic leaching of organic acids released by microbes (e.g., HCOOH). The process could likely be favored by the emergence of a pH gradient that would concentrate the bicarbonate in the outermost area of the biofilm. Such configuration would promote the precipitation and thickening of carbonates once the microbial attack is progressing.

interacting with FeS (e.g., pyrrothite) provide a simple chemical route to transfer electrons by the so-called pyrite-pulled reaction (Wächtershäuser 1992) following the geochemical pathway:

$$FeS + H_2S \rightarrow FeS_2 + H_2.$$

They would have easily operated in the Mars crust given its redox state, which has been estimated between ~1 log unit below fayalite-magnetite-quartz (FMQ) and ~1 log unit below iron-wustite (IW) (Sholes et al. 2017; Wadhwa 2008). QFM and IW correspond to mineral buffers of the interior of planetary bodies that partly control the composition of the volatiles released to the atmosphere (Ehlmann et al. 2016). These geochemical processes are more exergonic at pH below 6.5 and at an increasing temperature, which match with an acidic and thermophilic origin of life as discussed by Wächtershäuser (1992). Given the geochemical conditions of early Mars, the electron transfer mediated by S- and Fe-bearing compounds in the Mars crust could have certainly operated to provide the enough chemical energy to sustain an early metabolism. In this regard, the pyrite-pulled reaction would have played an essential role in the fixation of carbon. It would occur by the reduction of CO_2 that is a common volatile in different hydrothermal settings The CO_2 reduction through the mimic an incipient biochemical fixation of carbon (Wächtershäuser 1992, and references therein) in form of carboxylate ($HCOO^-$) as prebiotic precursor, followed by the generation of more reduced C-bearing compounds:

$$HCO_3^- + FeS + H_2S \rightarrow HCOO^- + FeS_2 + H_2O.$$
$$HCOO^- + FeS + H_2S + H^+ \rightarrow H_2CO + H_2O + FeS_2.$$

The emergence of a biogeochemical cycle could have started at the formation of carboxylate (Wächtershäuser 1992) and completed by the fixation of formaldehyde that is a building block for some essential biomolecules as sugars on early Earth (Cleaves 2008). This early biochemical cycle could have equally emerged in hydrothermal centers on Mars (Deamer and Damer 2017; Michalski et al. 2017), where redox state and geochemical composition enriched in S-, Fe-, and C-bearing compounds could have interplayed to form prebiotic precursors (Herschy et al. 2015; Lane and Martin 2012). Indeed, some biogeochemical pathways involved in the formation of mineral biosignatures in the Río Tinto basement resemble or are reverse to biochemical processes emerging in a Fe and S world (Wächtershäuser 1992). This is the case of the generation of HCO_3^- through the oxidation of organic compounds, when SRB metabolize sulfate bearing minerals like barite. Interestingly, such biogeochemical process is coupled to the formation of pyrite and hydrogen following the pyrite-pulled reaction. Consequently, the activity of a putative biosphere in the Mars subsurface should have been produced a mineral record comparable to the archive of secondary minerals produced by chemotrophic microbial activity in the Río Tinto subsurface.

The high concentration of sulfur and iron minerals in the crust of Mars suggests that they can sustain microbial communities through biogeochemical cycles propelled by differences in the redox conditions between the surface and subsurface (Fernández-Remolar et al. 2008). The extensive distribution of sulfates in the Mars surface (Grotzinger and Milliken 2012, and references therein) strongly supports that the planet had a reservoir with a sulfide-rich protolith that was later exposed to strong oxidation in the Hesperian (McCubbin et al. 2009; Gaillard et al. 2013). Under these conditions, microbial life could function through the biogeochemical cycling of sulfur and iron as a result of the redox difference between the upper oxidized crust and the deeper anoxic regions of the planet (Michalski et al. 2013). In this context, the structures and minerals described in this article would highlight the conditions and microbial processes that can occur in the Mars underground. Mars has experienced several hydrological cycles occurring in the early Noachian (Andrews-Hanna and Lewis 2011), during the late Noachian and early Hesperian that produced the network valleys (Di Achille and Hynek 2010), and in the late Hesperian to early Amazonian (Molina et al. 2017). During these hydric episodes water was abundant enough to interact with the martian crust. Under these conditions, sulfate and other ions

could have been easily mobilized and transported underground. In addition, different sulfate bearing minerals sourced in the Mars hydrothermal activity, as well as by diagenesis in sedimentary deposits (King and McLennan 2010; Vaniman et al. 2014) can provide the chemical disequilibrium in the subsurface to sustain sulfur-reducing microorganisms. Organic compounds and different ions could provide the energy source that would promote the reduction of sulfate in the subsurface. As discussed by Michalski et al. (2013), the main geochemical process occurring in the deep Mars crust of the southern highlands may have produced CH_4 and H_2 through serpentinization. As methane and other short-chained organics can be formed under hydrothermal conditions (Huber and Wächtershäuser 1997; Simoniet 2004), the underground biosphere of Mars could have used the C-bearing compounds as electron donors to reduce the sulfate minerals in the crust of Mars. In addition, the use of inorganic compounds (e.g., Fe^{2+}, H_2) as electron donors would also sustain a subsurface biosphere under the reduction of sulfate-bearing minerals. Under strong anoxic and alkaline conditions in the subsurface, down-welling acidic solutions enriched in sulfates would have provided the chemical disequilibrium through a strong geochemical gradient depending on pH and redox potential. This is, to some extent, the same configuration of the Río Tinto basement that is seasonally supplied by acidic meteoric solutions. Therefore, the use of methane, hydrogen, and short-chain organic compounds derived from serpentinization (Wang et al. 2014, and references therein) could have acted as an energy source for sulfur and iron microbial cycling. The sulfate groups in minerals like gypsum, anhydrite, and basanite, which are abundant mineral phases on Mars (Grotzinger and Milliken 2012; Nachon et al. 2014), could have acted as electron acceptors, mimicking the same process observed in barite in the Río Tinto. Whether or not the organic compounds would have been highly available to form carbonate-bearing biosignatures, the atmospheric and/or geological supply of CO_2 in the Mars subsurface would have been enough to promote carbonate formation. This would be favored under neutral to alkaline and anoxic conditions, which have been claimed for some potential underground habitats on Mars (Fernández-Remolar et al. 2008; Michalski et al. 2013). Furthermore, the existence of a cryptic biosphere fueled by mobilized ionic compounds from the upper lithosphere should be associated with the production of organic acid compounds that should concentrate in the Mars underground. Consequently, a high concentration of such materials in the subsurface could provide clear signs of microbial life in the Mars crust.

The emergence of chemotrophic life metabolizing S and Fe inorganic compounds is consistent with the early hydrothermal and volcanic activity, as well as the abundance of sulfur- and iron-bearing minerals in the Mars crust. It suggests that the Río Tinto-type mineral biosignatures that are formed through metabolizing S and Fe compounds in the subsurface can be useful in the search for extant and extinct subsurface life on the red planet. Furthermore, potential traces of life formed in the Mars underground would have greater chances to be preserved given they are protected against billions of years of watery activity interplaying with strong oxidizing and radiation conditions. Consequently, whether or not life existed on Mars, one first-class target to answer this essential question can be found in the subsurface. In the underground, a stable biosphere sustained by the iron and sulfur geochemical cycles could have risen and diversified. While in the planet surface, where conditions were changing and extreme, the environmental conditions were challenging for life.

Acknowledgments

This study was supported by the projects NRA-02-OSS-01 ASTEP Mars Astrobiology Research and Technology Experiment (MARTE) and Iberian Pyrite Belt Subsurface Life IPBSL (funded by the European Research Council) projects. The authors appreciate the strong support provided by the MARTE and IPBSL Science and Technology Teams. Authors are grateful for the ideas provided by Gordon Southam, Jeremiah Shuster, Javier Cuadros, Amy Williams, and one anonymous reviewer, who have greatly improved the manuscript.

References cited

Amaral Zettler, L.A., Gómez, F., Zettler, E., Keenan, B.G., Amils, R., and Sogin, M.L. (2002) Eukaryotic diversity in Spain's river of fire. Nature, 417, 137.

Amils, R., and Fernández-Remolar, D.C. (2014) Río Tinto: A geochemical and mineralogical terrestrial analogue of Mars. Life, 4, 511–534.

Amils, R., Fernández-Remolar, D.C., Parro, V., Rodríguez-Manfredi, J.A., Timmis, K., Oggerin, M., Sánchez-Román, M., López, F.J., Fernández, J.P., Puente, F., and others. (2013) Iberian Pyrite Belt Subsurface Life (IPBSL), a drilling project of biohydrometallurgical interest. Advanced Materials Research, 825, 15–18.

Andrews-Hanna, J.C., and Lewis, K.W. (2011) Early Mars hydrology: 2. Hydrological evolution in the Noachian and Hesperian epochs. Journal of Geophysical Research: Planets, 116, doi: 10.1029/2010JE003709.

Banfield, J.F., Moreau, J.W., Chan, C.S., Welch, S.A., and Little, B. (2001) Mineralogical biosignatures and the search for life on Mars. Astrobiology, 1, 447–465.

Barlow, N.G. (2008) Mars: An Introduction to Its Interior, Surface, and Atmosphere. Cambridge University Press.

Baumgartner, L.K., Reid, R.P., Dupraz, C., Decho, A.W., Buckley, D.H., Spear, J.R., Przekop, K.M., and Visscher, P.T. (2006) Sulfate reducing bacteria in microbial mats: Changing paradigms, new discoveries. Sedimentary Geology, 185, 131–145.

Bebié, J., and Schoonen, M.A.A. (2000) Pyrite surface interaction with selected organic aqueous species under anoxic conditions. Geochemical Transactions, 1(1), 47.

Bolze, C., Malone, P.G., and Smith, M.J. (1974) Microbial mobilization of barite. Chemical Geology, 13, 141–143.

Brocks, J.J., and Summons, R.E. (2003) Sedimentary hydrocarbons, biomarkers for early life. In W.H. Schlesinger, Ed., Treatise in Geochemistry, 8, p. 64–115. Elsevier.

Burton, E.D., Bush, R.T., Sullivan, L.A., and Mitchell, D.R.G. (2008) Schwertmannite transformation to goethite via the Fe(II) pathway: Reaction rates and implications for iron–sulfide formation. Geochimica et Cosmochimica Acta, 72, 4551–4564.

Castanier, S., Le Métayer-Levrel, G., and Perthuisot, J.-P. (1999) Ca-carbonates precipitation and limestone genesis—the microbiogeologist point of view. Sedimentary Geology, 126, 9–23.

Huber, C., and Wächtershäuser, G. (1997) Activated acetic acid by carbon fixation on (Fe,Ni)S under primordial conditions. Science, 276, 245.

Cleaves, H.J. (2008) The prebiotic geochemistry of formaldehyde. Precambrian Research, 164, 111–118.

Coupland, K., and Johnson, D.B. (2008) Evidence that the potential for dissimilatory ferric iron reduction is widespread among acidophilic heterotrophic bacteria. FEMS Microbiology Letters, 279, 30–35.

Crundwell, F.K. (2014) The mechanism of dissolution of minerals in acidic and alkaline solutions: Part II Application of a new theory to silicates, aluminosilicates and quartz. Hydrometallurgy, 149, 265–275.

Davis, R.A., Welty, A.T., Borrego, J., Morales, J.A., Pendon, J.G., and Ryan, J.G. (2000) Río Tinto estuary (Spain): 5000 years of pollution. Environmental Geology, 39, 1107–1116.

Deamer, D., and Damer, B. (2017) Can life begin on Enceladus? A perspective from hydrothermal chemistry. Astrobiology, 17, 834–839.

Di Achille, G., and Hynek, B.M. (2010) Ancient ocean on Mars supported by global distribution of deltas and valleys. Nature Geoscience, 3, 459–463.

Drobner, E., Huber, C., Wächtershäuser, G., Rose, D., and Stetter, K.O. (1990) Pyrite formation linked with hydrogen evolution under anaerobic conditions. Nature, 346, 742–744.

Edwards, K.J., Goebel, B.M., Rodgers, T.M., Schrenk, M.O., Gihring, T.M., Cardona, M.M., Mcguire, M.M., Hamers, R.J., Pace, N.R., and Bandfield, J.F. (1999) Geomicrobiology of pyrite (FeS_2) dissolution: Case study at Iron Mountain, California. Geomicrobiology Journal, 16, 155–179.

Ehlmann, B.L., Anderson, F.S., Andrews-Hanna, J., Catling, D.C., Christensen, P.R., Cohen, B.A., Dressing, C.D., Edwards, C.S., Elkins-Tanton, L.T., Farley, K.A., and others. (2016) The sustainability of habitability on terrestrial planets: Insights, questions, and needed measurements from Mars for understanding the evolution of Earth-like worlds. Journal of Geophysical Research: Planets, 121, 1927–1961.

Essalhi, M., Sizaret, S., Barbanson, L., Chen, Y., Lagroix, F., Demory, F., Nieto, J., Sáez, R., and Capitán, M.Á. (2011) A case study of the internal structures of gossans and weathering processes in the Iberian Pyrite Belt using magnetic fabrics and paleomagnetic dating. Mineralium Deposita, 46, 981–999.

Fernández-Remolar, D., Rodríguez, N., Gómez, F., and Amils, R. (2003) The geological record of an acidic environment driven by iron hydrochemistry: The Tinto River system. Journal of Geophysical Research, 108, doi: 10.1029/2002JE001918.
Fernández-Remolar, D.C., Morris, R.V., Gruener, J.E., Amils, R., and Knoll, A.H. (2005) The Río Tinto Basin, Spain: Mineralogy, sedimentary geobiology, and implications for interpretation of outcrop rocks at Meridiani Planum, Mars. Earth and Planetary Science Letters, 240, 149–167.
Fernández-Remolar, D.C., Prieto-Ballesteros, O., Rodríguez, N., Gómez, F., Amils, R., Gómez-Elvira, J., and Stoker, C.R. (2008) Underground habitats in the Río Tinto Basin: A model for subsurface life habitats on Mars. Astrobiology, 8, 1023–1047.
Fernández-Remolar, D.C., Prieto-Ballesteros, O., Gómez-Ortíz, D., Fernández-Sampedro, M., Sarrazin, P., Gailhanou, M., and Amils, R. (2011) Río Tinto sedimentary mineral assemblages: A terrestrial perspective that suggests some formation pathways of phyllosilicates on Mars. Icarus, 211, 114–138.
Fernández-Remolar, D.C., Preston, L.J., Sánchez-Román, M., Izawa, M.R.M., Huang, L., Southam, G., Banerjee, N.R., Osinski, G.R., Flemming, R., Gómez-Ortíz, D., and others. (2012) Carbonate precipitation under bulk acidic conditions as a potential biosignature for searching life on Mars. Earth and Planetary Science Letters, 351, 13–26.
Gaillard, F., Michalski, J., Berger, G., McLennan, S.M., and Scaillet, B. (2013) Geochemical reservoirs and timing of sulfur cycling on Mars. Space Science Reviews, 174, 251–300.
García-Moyano, A., González-Toril, E., Aguilera, Á., and Amils, R. (2012) Comparative microbial ecology study of the sediments and the water column of the Río Tinto, an extreme acidic environment. FEMS Microbiology Ecology, 81(2), 303–314.
Goldstein, J., Newbury, D.E., Joy, D.C., Lyman, C.E., Echlin, P., Lifshin, E., Sawyer, L., and Michael, J.R. (2003) Scanning Electron Microscopy and X-ray Microanalysis. Springer, New York.
Gómez-Ortiz, D., Fernández-Remolar, D.C., Granda, Á., Quesada, C., Granda, T., Prieto-Ballesteros, O., Molina, A., and Amils, R. (2014) Identification of the subsurface sulfide bodies responsible for acidity in Río Tinto source water, Spain. Earth and Planetary Science Letters, 391, 36–41.
González-Toril, E.F., Llobet-Brossa, E., Casamayor, E.O., Amann, R., and Amils, R. (2003) Microbial ecology of an extreme acidic environment, the Tinto River. Applied and Environmental Microbiology, 69, 4853–4865.
Grotzinger, J.P., and Milliken, R.E. (2012) The Sedimentary Rock Record of Mars. Sedimentary Geology of Mars, 102, 1–48. SEPM Society for Sedimentary Geology.
Herschy, B., Whicher, A., Camprubi, E., Watson, C., Dartnell, L., Ward, J., Evans, J.R.G., and Lane, N. (2014) An origin-of-life reactor to simulate alkaline hydrothermal vents. Journal of Molecular Evolution, 79, 213–227.
King, P.L., and McLennan, S.M. (2010) Sulfur on Mars. Elements, 6, 107.
Knoll, A.H., Canfield, D.E., and Konhauser, K.O. (2012) Fundamentals of Geobiology. Blackwell, Oxford, U.K.
Lane, N., and Martin, W.F. (2012) The origin of membrane bioenergetics. Cell, 151, 1406–1416.
Leistel, J.M., Marcoux, E., Thiéblemont, D., Quesada, C., Sánchez, A., Almodóvar, G.R., Pascual, E., and Sáez, R. (1998) The volcanic-hosted massive sulphide deposits of the Iberian Pyrite Belt. Mineralium Deposita, 33, 2–30.
Leybourne, M.I., Hamilton, S.M., Mwenifumbo, C.J., Goodfellow, W.D., and Boyle, D.R. (2009) Hydrogeochemical and geophysical evidence for borehole oxidation of massive sulphides below the water table and generation of self-potential anomalies. Geochemistry: Exploration, Environment, Analysis, 9, 39–50.
López-Archilla, A.I., González, A.E., Terrón, M.C., and Amils, R. (2005) Diversity and ecological relationships of the fungal populations of an acidic river of Southwestern Spain: The Tinto River. Canadian Journal of Microbiology, 50, 923–934.
Malki, M., González-Toril, E., Sanz, J.L., Gómez, F., Rodríguez, N., and Amils, R. (2006) Importance of the iron cycle in biohydrometallurgy. Hydrometallurgy, 83, 223–228.
Malki, M., de Lacey, A.L., Rodríguez, N., Amils, R., and Fernandez, V.M. (2008) Preferential use of an anode as an electron acceptor by an acidophilic bacterium in the presence of oxygen. Applied and Environmental Microbiology, 74, 4472–4476.
McCubbin, F.M., Tosca, N.J., Smirnov, A., Nekvasil, H., Steele, A., Fries, M., and Lindsley, D.H. (2009) Hydrothermal jarosite and hematite in a pyroxene-hosted melt inclusion in martian meteorite Miller Range (MIL) 03346: Implications for magmatic-hydrothermal fluids on Mars. Geochimica et Cosmochimica Acta, 73, 4907–4917.
Michalski, J.R., Cuadros, J., Niles, P.B., Parnell, J., Deanne Rogers, A., and Wright, S.P. (2013) Groundwater activity on Mars and implications for a deep biosphere. Nature Geoscience, 6, 133–138.
Michalski, J.R., Dobrea, E.Z.N., Niles, P.B., and Cuadros, J. (2017) Ancient hydrothermal seafloor deposits in Eridania basin on Mars. Nature Communications, 8, 15978.
Molina, A., López, I., Prieto-Ballesteros, O., Fernández-Remolar, D., de Pablo, M.Á, and Gómez, F. (2017) Coogoon Valles, western Arabia Terra: Hydrological evolution of a complex martian channel system. Icarus, 293 (Supplement C), 27–44.
Nachon, M., Clegg, S.M., Mangold, N., Schröder, S., Kah, L.C., Dromart, G., Ollila, A., Johnson, J.R., Oehler, D.Z., Bridges, J.C., and others. (2014) Calcium sulfate veins characterized by ChemCam/Curiosity at Gale crater, Mars. Journal of Geophysical Research: Planets, 119, 1991–2016.
Nordstrom, D.K., Alpers, C.N., Ptacek, C.J., and Blowes, D.W. (2000) Negative pH and extremely acidic mine waters from Iron Mountain, California. Environmental Science & Technology, 34, 254–258.
Oggerin, M., Tornos, F., Rodríguez, N., De Moral, C., and Sánchez-Román, M. (2013) Specific jarosite biomineralization by *Purpureocillium lilacinum*, an acidophilic fungi isolated from Río Tinto. Environmental Microbiology, 15, 2228–2237.
Ohmura, N., Sasaki, K., Matsumoto, N., and Saiki, H. (2002) Anaerobic respiration using Fe^{3+}, S^0 and H_2 in the chemolithoautotrophic bacterium. Journal of Bacteriology, 18, 2081–2087.
Oliveira, J.T. (1990) Stratigraphy and syn-sedimentary tectonism in the South Portuguese Zone. In R.D. Dallmeyer, and E. Martínez García, Eds., Pre-Mesozoic Geology of Iberia, p. 334–347. Springer, Berlin.
Parro, V., Fernández-Calvo, P., Rodríguez Manfredi, J.A., Moreno-Paz, M., Rivas, L.A., García-Villadangos, M., Bonaccorsi, R., González-Pastor, J.E., Prieto-Ballesteros, O., Schuerger, A.C., Davidson, M., Gómez-Elvira, J., and Stoker, C.R. (2008) SOLID2: An antibody array-based life-detector instrument in a Mars Drilling Simulation Experiment (MARTE). Astrobiology, 8, 987–999.
Peretyazhko, T., Zachara, J.M., Boily, J.F., Xia, Y., Gassman, P.L., Arey, B.W., and Burgos, W.D. (2009) Mineralogical transformations controlling acid mine drainage chemistry. Chemical Geology, 262, 169–178.
Puente-Sánchez, F., Moreno-Paz, M., Rivas, L.A., Cruz-Gil, P., García-Villadangos, M., Gómez, M.J., Postigo, M., Garrido, P., González-Toril, E., Briones, C., and others. (2014) Deep subsurface sulfate reduction and methanogenesis in the Iberian Pyrite Belt revealed through geochemistry and molecular biomarkers. Geobiology, 12, 34–47.
Quesada, C. (1991) Geological constraints on the Paleozoic tectonic evolution of tectonostratigraphic terranes in the Iberian Massif. Tectonophysics, 185, 225–245.
——— (1998) A reappraisal of the structure of the Spanish segment of the Iberian Pyrite Belt. Mineralium Deposita, 33, 31–44.
Rickard, D., and Luther, G.W. (2007) Chemistry of iron sulfides. Chemical Reviews, 107, 514–562.
Rodriguez-Navarro, C., Jroundi, F., Schiro, M., Ruiz-Agudo, E., and González-Muñoz, M.T. (2012) Influence of substrate mineralogy on bacterial mineralization of calcium carbonate: Implications for stone conservation. Applied and Environmental Microbiology, 78, 4017–4029.
Sánchez-Andrea, I., Rodríguez, N., Amils, R., and Sanz, J.L. (2011) Microbial diversity in anaerobic sediments at Río Tinto, a naturally acidic environment with a high heavy metal content. Applied and Environmental Microbiology, 77, 6085–6093.
Sánchez-Román, M., Puente-Sánchez, F., Parro, V., and Amils, R. (2015) Nucleation of Fe-rich phosphates and carbonates on microbial cells and exopolymeric substances. Frontiers in Microbiology, 6, 1024.
Sand, W., Gehrke, T., Jozsa, P.-G., and Schippers, A. (2001) (Bio)chemistry of bacterial leaching–direct vs. indirect bioleaching. Hydrometallurgy, 59, 159–175.
Sholes, S.F., Smith, M.L., Claire, M.W., Zahnle, K.J., and Catling, D.C. (2017) Anoxic atmospheres on Mars driven by volcanism: Implications for past environments and life. Icarus, 290, 46–62.
Simoneit, B.R.T. (2004) Prebiotic organic synthesis under hydrothermal conditions: An overview. Advances in Space Research, 33, 88–94.
Stoker, C.R., Cannon, H.N., Dunagan, S.E., Lemke, L.G., Glass, B.J., Miller, D., Gomez-Elvira, J., Davis, K., Zavaleta, J., Winterholler, A., and others. (2008) The 2005 MARTE Robotic Drilling Experiment in Río Tinto, Spain: Objectives, approach, and results of a simulated mission to search for life in the martian subsurface. Astrobiology, 8, 921–945.
Uwins, P.J.R., Webb, R.I., and Taylor, A.P. (1998) Novel nano-organisms from Australian sandstones. American Mineralogist, 83, 1541–1550.
Vaniman, D.T., Bish, D.L., Ming, D.W., Bristow, T.F., Morris, R.V., Blake, D.F., Chipera, S.J., Morrison, S.M., Treiman, A.H., Rampe, E.B., and others. (2014) Mineralogy of a Mudstone at Yellowknife Bay, Gale Crater, Mars. Science, 343(6169).
Wächtershäuser, G. (1992) Groundworks for an evolutionary biochemistry: The iron-sulphur world. Progress in Biophysics and Molecular Biology, 58, 85–201.
Wadhwa, M. (2008) Redox conditions on small bodies, the Moon and Mars. Reviews in Mineralogy and Geochemistry, 68, 493–510.
Wang, X., Ouyang, Z., Zhuo, S., Zhang, M., Zheng, G., and Wang, Y. (2014) Serpentinization, abiogenic organic compounds, and deep life. Science China Earth Sciences, 57, 878–887.
Welch, S.A., and Vandevivere, P. (1994) Effect of microbial and other naturally occurring polymers on mineral dissolution. Geomicrobiology Journal, 12, 227–238.
Zhou, Y., Wang, R., and Lu, X. (2011) Anorthite dissolution promoted by bacterial adhesion: Direct evidence from dialytic experiment. Science China Earth Sciences, 54, 204–211.
Zhu, T., and Dittrich, M. (2016) Carbonate precipitation through microbial activities in natural environment, and their potential in biotechnology: A review. Frontiers in Bioengineering and Biotechnology, 4, 4.

Manuscript received August 28, 2017
Manuscript accepted December 8, 2017
Manuscript handled by Javier Cuadros

Endnote:

[1]Deposit item AM-18-36288, Supplemental Figures. Deposit items are free to all readers and found on the MSA web site, via the specific issue's Table of Contents (go to http://www.minsocam.org/MSA/AmMin/TOC/2018/Mar2018_data/Mar2018_data.html).